Journal of Scientific Computing (2023) 94:26
https://doi.org/10.1007/s10915-022-02079-0

Locking-Free and Locally-Conservative Enriched Galerkin Method for Poroelasticity

Sanghyun Lee[1] · **Son-Young Yi**[2]

Received: 16 April 2022 / Revised: 2 December 2022 / Accepted: 12 December 2022

Abstract
This paper develops a new coupled enriched Galerkin (EG) scheme for Biot's poroelasticity model based on the displacement-pressure formulation. The aim of this work is to provide a stable and robust numerical method for a wide range of physical and numerical parameters. The finite-dimensional solution spaces are enriched linear Lagrange spaces, and the inf-sup condition between the two spaces is achieved by adding a stabilization term. The resulting coupled EG method is locally conservative and provides stable solutions without spurious oscillations or overshoots/undershoots. The well-posedness and optimal a priori error estimates are established. Numerical results in various scenarios are provided.

Keywords Biot · Poroelasticity · Enriched Galerkin · Locking-free · Local mass conservation

Mathematics Subject Classification 65M60 · 74F10

1 Introduction

The deformation of a solid porous material caused by the change of fluid pressure inside the material may cause the change in permeability and porosity of the porous material, which in turn affects the fluid pressure. These coupled processes between the fluid flow and solid deformation are commonly modeled by Biot's system of poroelasticity equations [5, 6]. Biot's system consists of two partial differential equations, describing the conservation of momentum for the solid mechanics and the conservation of mass for the fluid flow. This model has been employed to model various applications in science and engineering fields, including

✉ Son-Young Yi
syi@utep.edu

Sanghyun Lee
lee@math.fsu.edu

[1] Department of Mathematics, Florida State University, Tallahassee, FL 32306, USA

[2] Department of Mathematical Sciences, University of Texas at El Paso, El Paso TX, 79968, USA

Published online: 29 December 2022

groundwater contamination, fossil fuel production, earthquake mechanics, geothermal energy harvest, and biomedical engineering.

While various numerical methods (e.g., finite difference [4, 26, 27] and finite volume [15, 31, 38] methods) have been employed to solve Biot's equations, the most popular methods fall into the category of general finite element methods (FEMs) [12, 17–19, 21, 25, 28, 43–46]. In particular, it is a common practice to couple different types of FEMs tailored for each subproblem, mechanics or flow, to satisfy the underlying physical law or to overcome the known numerical difficulties associated with each governing equation. Some examples include the coupling of continuous Galerkin (CG) and mixed finite element method (MFEM) [33, 44, 46], discontinuous Galerkin (DG) and MFEM [34], MFEM and MFEM [2, 3, 45], and CG and enriched Galerkin (EG) method [12, 19].

There are several numerical challenges when solving poroelasticity problems. First of all, regardless of what combination of numerical methods is used, the choice of the finite-dimensional solution spaces cannot be made independently of one another. As is well-known for mixed finite element methods, the solution spaces should be inf-sup stable [7, 9]. The violation of this stability condition in the poroelasticity modeling may result in spurious pressure oscillations, known as *pressure locking*, for a certain range of material and numerical parameters [8, 35, 36, 46]. Overcoming pressure locking has been a subject of extensive research in the past couple of decades [14, 24, 29, 34, 42, 45, 46].

However, the lack of the inf-sup condition is not the only cause of pressure oscillations in poroelasticity simulations. In other words, the inf-sup stability does not necessarily guarantee oscillation-free pressure solutions, in particular, near material interfaces with high contrast permeability values. A good example of an inf-sup stable element that presents pressure oscillations in heterogeneous media is the Taylor-Hood element [28, 41]. Indeed, these oscillations (overshoots/undershoots) are related to the lack of local mass conservation in the numerical method. Therefore, they should be distinguished from the pressure locking phenomenon. The aim of this research is to provide a numerical method that is free of both types of pressure oscillations.

In this present work, we propose a coupled EG method for solving the Biot model, where we solve both the mechanics and flow problems using EG methods. The EG method is a new class of FEMs that combines the advantages of the two most extensively studied FEMs: CG and DG methods. The EG solution space is obtained by enriching a CG space with a minimal set of suitable discontinuous functions to achieve some desired properties that the CG method lacks, for example, local mass conservation. On the other hand, the non-conformity of the solution space is accounted for by using a DG-like weak formulation. Therefore, the computational cost for the EG method is much lower than the DG method due to the fewer degrees of freedom (DOFs) and a simpler sparse linear system. Moreover, one can utilize existing CG and DG codes to implement the EG method with some slight modifications.

In our new coupled EG method, we employ the linear CG space enriched by piecewise constants for the pressure solution. This EG space was employed in [20, 22, 23, 39] to study coupled flow and transport problems in porous media. The resulting EG method for the flow equation provides local mass conservation and yields solutions with no spurious oscillations, which would normally be present if the CG method was used, in heterogeneous porous media. For the displacement space, we enrich the linear vector-valued CG space with an enrichment space spanned by one local linear basis function per element. This EG space was utilized by the authors in [47, 48] for simulating nearly incompressible elastic materials and incompressible Stokes flow. On the other hand, the temporal discretization is done using the backward Euler method for simple analysis. Another important aspect of our EG method is the presence of a stabilization term, which plays an essential role in achieving

the inf-sup condition and provide oscillation-free solutions. We prove the well-posedness and optimal a priori error estimates for the new method. Also, we demonstrate through several numerical experiments that our coupled EG method yields oscillation-free solutions for problems in various scenarios, where we would normally observe pressure locking or overshoots/undershoots when solved by CG methods. Recently, a five-field MFEM for the Biot model that enjoys similar properties to ours was presented in [2]. Though their original method requires the solution of a much larger linear system than ours, the method can be reduced to a cheap ($\mathbb{P}_0$-$\mathbb{P}_0$) pressure-displacement system, whose reduction process involves the solution of local problems.

The outline of the rest of the paper is as follows. We start with presenting the governing equations in Sect. 2 and introducing some useful notations in Sect. 3. Then, we define our EG method and show its mass conservation property in Sects. 4 and 5, respectively. The next two sections, Sects. 6 and 7, are dedicated to prove the well-posedness and optimal a priori error estimates. Finally, in Sect. 8, we present the numerical results of our numerical experiments.

2 Governing Equations

Let Ω be a bounded, connected, Lipschitz domain in $\mathbb{R}^d$, $d = 2, 3$, and let $\mathbb{I} = (0, T_f]$ with $T_f > 0$. Also, let $\mathbf{u}$ be the displacement of the solid phase and p be the fluid pressure. Then, the governing equations are

$$-\nabla \cdot (\boldsymbol{\sigma}(\mathbf{u}) - \alpha p \mathbf{I}) = \mathbf{f} \quad \text{in } \Omega \times \mathbb{I}, \tag{1a}$$

$$\frac{\partial}{\partial t}(c_0 p + \alpha \nabla \cdot \mathbf{u}) - \nabla \cdot (\mathbf{K} \nabla p) = g \quad \text{in } \Omega \times \mathbb{I}, \tag{1b}$$

where $\mathbf{f}$ is the body force and g is the volumetric source/sink term. Also, $\boldsymbol{\sigma}$ is the standard stress tensor from linear elasticity, satisfying the constitutive equation $\boldsymbol{\sigma}(\mathbf{u}) = 2\mu\boldsymbol{\epsilon}(\mathbf{u}) + \lambda(\nabla \cdot \mathbf{u})\mathbf{I}$, where $\boldsymbol{\epsilon}(\mathbf{u}) = \frac{1}{2}[\nabla \mathbf{u} + (\nabla \mathbf{u})^T]$ is the strain tensor, $\mathbf{I}$ is the $d \times d$ identity tensor, and μ, λ are the Lamé constants. The Lamé constants are assumed to be in the range $[\mu_0, \mu_1] \times [0, \infty)$ for some $0 < \mu_0 < \mu_1 < \infty$. Then, the total stress tensor is given by $\tilde{\boldsymbol{\sigma}} = \boldsymbol{\sigma} - \alpha p \mathbf{I}$, where α is the *Biot-Willis* constant. The momentum balance for the fluid is interpreted as the Darcy law for the volumetric fluid flux: $\mathbf{q} = -\mathbf{K}\nabla p$. We ignore the gravity effect here for a simple presentation of the numerical method. However, it is straightforward to include the gravity term in the numerical formulation. The permeability tensor, $\mathbf{K} \in \mathbb{R}^{d \times d}$, is a symmetric and uniformly positive definite tensor satisfying the following assumption: there exist positive constants $k_{\min}$ and $k_{\max}$ such that for any $\mathbf{x} \in \Omega$,

$$k_{\min} \boldsymbol{\xi}^T \boldsymbol{\xi} \leq \boldsymbol{\xi}^T \mathbf{K}(\mathbf{x}) \boldsymbol{\xi} \leq k_{\max} \boldsymbol{\xi}^T \boldsymbol{\xi}, \quad \forall \boldsymbol{\xi} \in \mathbb{R}^d.$$

The fluid content, η, can be written as $\eta = c_0 p + \alpha \nabla \cdot \mathbf{u}$, where c_0 is the constrained specific storage coefficient. The mass conservation states that $\eta_t = -\nabla \cdot \mathbf{q} + g$.

To complete the system (1), we have to prescribe suitable boundary and initial conditions. To this end, we introduce two pairs of partitions of the boundary of Ω, $\{\Gamma_p, \Gamma_f\}$ and $\{\Gamma_d, \Gamma_t\}$, such that $\partial\Omega = \overline{\Gamma_p} \cup \overline{\Gamma_f}$ and $\partial\Omega = \overline{\Gamma_d} \cup \overline{\Gamma_t}$. In this paper, we assume that $|\Gamma_p| > 0$ and $|\Gamma_d| > 0$. Then, we prescribe the following mixed boundary conditions:

$$p = p_D \text{ on } \Gamma_p, \quad (\mathbf{K}\nabla p) \cdot \mathbf{n} = q_N \text{ on } \Gamma_f, \quad \mathbf{u} = \mathbf{u}_D \text{ on } \Gamma_d, \quad \tilde{\boldsymbol{\sigma}}\mathbf{n} = \mathbf{t}_N \text{ on } \Gamma_t, \tag{2}$$

where $\mathbf{n}$ is the outward unit normal vector. We also have the following initial conditions:

$$p(\cdot, 0) = p^0 \text{ and } \mathbf{u}(\cdot, 0) = \mathbf{u}^0 \text{ in } \Omega \tag{3}$$

such that

$$p^0 = p_D(\cdot, 0) \text{ on } \Gamma_p \quad \text{and} \quad \mathbf{u}^0 = \mathbf{u}_D(\cdot, 0) \text{ on } \Gamma_d.$$

The existence, uniqueness, and regularity theory of the solution of the governing equations (1) is developed in [37].

3 Notation and Preliminaries

In this section, we introduce some notations and preliminaries that will be useful throughout the rest of the paper. We adopt standard notations for Sobolev spaces $H^s(E)$ [1] and their associated inner products $(\cdot, \cdot)_E$, norms $\|\cdot\|_{s,E}$, and seminorms $|\cdot|_{s,E}$ on a subdomain $E \subseteq \mathbb{R}^d$. We extend these definitions and notations naturally to vector functions $\boldsymbol{\zeta} : E \to \mathbb{R}^d$ and tensor functions $\boldsymbol{\tau} : E \to \mathbb{R}^{d\times d}$. When $s = 0$, $H^s(E)$ coincides with $L^2(E)$. In this case, the inner product will be denoted by $(\cdot, \cdot)_E$. For simplicity, the subscript E will be dropped if $E = \Omega$. For vector functions $\mathbf{v}, \mathbf{w} \in [L^2(E)]^d$, the notation $(\mathbf{v}, \mathbf{w})_E$ denotes the integral of their dot product over E, and for tensor functions $\boldsymbol{\tau}, \boldsymbol{\omega} \in [L^2(E)]^{d\times d}$, the same notation denotes the integral of the Frobenius inner product $\boldsymbol{\tau} : \boldsymbol{\omega} := tr(\boldsymbol{\tau}^T \boldsymbol{\omega})$. If $E \subseteq \mathbb{R}^{d-1}$, then the innder product will be denoted by $\langle \cdot, \cdot \rangle_E$. For any subset $\Gamma \subseteq \partial\Omega$, $H^s_{0,\Gamma}(\Omega) = \{w \in H^s(\Omega) \mid w = 0 \text{ on } \Gamma\}$.

Let $\mathcal{T}_h$ be a shape-regular triangulation by a family of partitions of Ω into elements K, where K is a triangle when $d = 2$ and a tetrahedron when $d = 3$. We denote by h_K the diameter of K and we set $h = \max_{K\in\mathcal{T}_h} h_K$. Also, we denote by $\mathcal{E}_h$ the set of all edges (or faces) and by $\mathcal{E}_h^I$ the collection of all interior edges (faces), respectively. For any $e \in \mathcal{E}_h^I$, there are two neighboring elements K^+ and K^- such that $e = \partial K^+ \cap \partial K^-$. We associate one unit normal vector $\mathbf{n}_e$ with e, which is assumed to be oriented from K^+ to K^-. If $e \in \mathcal{E}_h^b := \mathcal{E}_h \setminus \mathcal{E}_h^I$, then $\mathbf{n}_e$ is taken to be the outward unit normal vector to $\partial\Omega$.

The development of an EG method requires broken Sobolev spaces, which depend on the partition of the domain. The broken Sobolev space $H^s(\mathcal{T}_h)$ for any real number s is defined by $H^s(\mathcal{T}_h) = \{v \in L^2(\Omega) \mid v|_K \in H^s(K) \ \forall K \in \mathcal{T}_h\}$, equipped with the broken inner product $(w, q)_{\mathcal{T}_h} = \sum_{K\in\mathcal{T}_h} (w, q)_K$ and a broken Sobolev norm $\|w\|_{H^s(\mathcal{T}_h)} = \left(\sum_{K\in\mathcal{T}_h} \|w\|_{s,K}\right)^{\frac{1}{2}}$. Similarly, $L^2(\mathcal{E}_h)$ refers to the set of functions whose traces on the elements of $\mathcal{E}_h$ are square-integrable. This space is equipped with the broken inner product $(w, q)_{\mathcal{E}_h} = \sum_{e\in\mathcal{E}_h} \langle w, q\rangle_e$ and a broken Sobolev norm $\|w\|_{H^s(\mathcal{E}_h)} = \left(\sum_{e\in\mathcal{E}_h} \|w\|_{s,e}\right)^{\frac{1}{2}}$. These definitions and notations can be naturally extended to vector and tensor functions.

For $\boldsymbol{\zeta} \in [H^1(\mathcal{T}_h)]^d$, the trace of $\boldsymbol{\zeta}$ along ∂K for any element K is well defined. If $e \in \mathcal{E}_h^I$ is shared by two elements K^+ and K^-, there are two traces of $\boldsymbol{\zeta}$ on e, which will be denoted by $\boldsymbol{\zeta}^\pm$, respectively. Now, we introduce the so-called average and jump operators, $\{\cdot\}$ and $[\![\cdot]\!]$, respectively, as follows:

$$\begin{cases} \{\boldsymbol{\zeta}\} := \frac{1}{2}\left(\boldsymbol{\zeta}^+ + \boldsymbol{\zeta}^-\right) \text{ and } [\![\boldsymbol{\zeta}]\!] := \left(\boldsymbol{\zeta}^+ - \boldsymbol{\zeta}^-\right) & \text{if } e \in \mathcal{E}_h^I, \\ \{\boldsymbol{\zeta}\} = [\![\boldsymbol{\zeta}]\!] := \boldsymbol{\zeta} & \text{if } e \in \mathcal{E}_h^b. \end{cases}$$

We use the same definitions and notation for vector and tensor functions.

Lastly, we recall important trace inequalities that will be frequently used in the analysis of our EG method. Let $|K|$ denote the area of K in two dimensions and the volume of K in three dimensions. Similarly, $|e|$ denotes the length of e in two dimensions and the area of e in three dimensions. Then, there is a constant C_t independent of h_K and v such that for any $v \in H^s(K)$, $s \geq 1$,

$$\|v\|_{0,e} \leq C_t |e|^{1/2} |K|^{-1/2} (\|v\|_{0,K} + h_K \|\nabla v\|_{0,K}) \quad \forall e \subset \partial K. \tag{4}$$

If $v \in \mathbb{P}_k(K)$, where $\mathbb{P}_k(K)$ is the space of polynomials of total degree at most k, then the trace inequality becomes

$$\|v\|_{0,e} \leq \tilde{C}_t |e|^{1/2} |K|^{-1/2} \|v\|_{0,K} \quad \forall e \subset \partial K, \tag{5}$$

where $\tilde{C}_t$ is independent of h_K and v but depends on the polynomial degree k. We note that analogous inequalities to (4) and (5) hold for vector and tensor functions.

4 Variational Formulation and Enriched Galerkin Method

In this section, we derive a variational formulation for the model problem (1) and propose a fully-discrete EG method. In order to derive a variational problem, we multiply (1a) and (1b) by $\mathbf{v} \in [H^1_{0,\Gamma_d}(\Omega)]^d$ and $w \in H^1_{0,\Gamma_p}(\Omega)$, respectively, and integrate by parts. Then, the resulting variational formulation reads as follows: At every $t \in (0, T_f]$, find $(\mathbf{u}, p) \in [H^1(\Omega)]^d \times H^1(\Omega)$ such that $\mathbf{u} = \mathbf{u}_D$ on Γ_d and $p = p_D$ on Γ_p and satisfy

$$\mathbf{a}^{\mathbf{u}}(\mathbf{u}, \mathbf{v}) - \alpha(p, \nabla \cdot \mathbf{v}) = (\mathbf{f}, \mathbf{v}) + (\mathbf{t}_N, \mathbf{v})_{\Gamma_t} \qquad \forall \mathbf{v} \in [H^1_{0,\Gamma_d}(\Omega)]^d, \tag{6a}$$

$$c_0(p_t, w) + \alpha(\nabla \cdot \mathbf{u}_t, w) + \mathbf{a}^p(p, w) = (g, w) + (q_N, w)_{\Gamma_f} \qquad \forall w \in H^1_{0,\Gamma_p}(\Omega), \tag{6b}$$

where the bilinear forms $\mathbf{a}^{\mathbf{u}}(\mathbf{u}, \mathbf{v})$ and $\mathbf{a}^p(p, w)$ are defined by

$$\mathbf{a}^{\mathbf{u}}(\mathbf{u}, \mathbf{v}) = 2\mu(\varepsilon(\mathbf{u}), \varepsilon(\mathbf{v})) + \lambda(\nabla \cdot \mathbf{u}, \nabla \cdot \mathbf{v}) \qquad \forall \mathbf{u}, \mathbf{v} \in [H^1(\Omega)]^d$$

$$\mathbf{a}^p(p, w) = (\mathbf{K}\nabla p, \nabla w) \qquad \forall p, w \in H^1(\Omega).$$

It is trivial to see that $\mathbf{a}^{\mathbf{u}}(\cdot, \cdot)$ is symmetric and continuous. Given that $|\Gamma_d| > 0$, the second Korn's inequality holds on $[H^1_{0,\Gamma_d}(\Omega)]^d$ [30]. In other words, there exists $C = C(\Omega, \Gamma_d) > 0$ such that

$$\|\mathbf{v}\|_1 \leq C \|\varepsilon(\mathbf{v})\|_0, \quad \forall \mathbf{v} \in [H^1_{0,\Gamma_d}(\Omega)]^d. \tag{7}$$

Therefore, $\mathbf{a}^{\mathbf{u}}(\cdot, \cdot)$ is coercive on $[H^1_{0,\Gamma_d}(\Omega)]^d$.

For the spatial discretization of the weak form (6), let us introduce our EG finite element spaces for the displacement and pressure on a shape-regular mesh $\mathcal{T}_h$. Let $\mathcal{C}_h$ be the standard linear CG finite element space and $\boldsymbol{\mathcal{C}}_h = (\mathcal{C}_h)^d \subset [H^1(\Omega)]^d$ be the vector-valued linear CG space. Also, let

$$\boldsymbol{\mathcal{D}}^{\mathbf{u}}_h = \left\{ \psi \in [L^2(\Omega)]^d \mid \psi|_K = c_K(\mathbf{x} - \mathbf{x}_K), \quad c_K \in \mathbb{R} \ \forall K \in \mathcal{T}_h \right\},$$

where $\mathbf{x} = [x_1, \cdots, x_d]^T$ and $\mathbf{x}_K$ is the position vector of the center of $K \in \mathcal{T}_h$, that is, $(\mathbf{x} - \mathbf{x}_K, 1)_K = 0$. Then, the EG finite element space for the displacement is defined as

$$\boldsymbol{\mathcal{V}}_{\boldsymbol{h}} := \boldsymbol{\mathcal{C}}_h \oplus \boldsymbol{\mathcal{D}}^{\mathbf{u}}_h,$$

where the direct sum can be established because $\boldsymbol{\mathcal{C}}_h \cap \boldsymbol{\mathcal{D}}_h^{\mathbf{u}} = \{\mathbf{v} \mid \mathbf{v} \equiv \mathbf{0} \text{ on } \Omega\}$. For the pressure space, first let

$$\mathcal{D}_h^p = \left\{\psi \in L^2(\Omega) \mid \psi|_K \in \mathbb{P}_0(K) \quad \forall K \in \mathcal{T}_h\right\}.$$

Then, the space for the pressure is defined as

$$\mathcal{W}_h := \mathcal{C}_h + \mathcal{D}_h^p.$$

Note that $\mathcal{W}_h$ is not a direct sum unlike $\boldsymbol{\mathcal{V}_h}$. Also, both $\boldsymbol{\mathcal{V}_h}$ and $\mathcal{W}_h$ require only one additional local degree of freedom per element compared to the linear CG spaces $\boldsymbol{\mathcal{C}}_h$ and $\mathcal{C}_h$, respectively, regardless of the dimension d.

To discretize (6) in time, we employ the backward Euler method for simplicity. However, higher-order time-stepping methods can be also considered in practice to achieve the same convergence orders in space and time. For a positive integer N, $\Delta t = T_f/N$ is the time step and $t^n = n\Delta t$. For any known function $\phi(t)$, the function value at time t^n is denoted by ϕ^n. That is, $\phi^n = \phi(t^n)$. In our EG method, $(\mathbf{u}_h^n, p_h^n)$ is an approximation of $(\mathbf{u}^n, p^n)$, where $n = 0, \ldots, N$.

Finally, our fully-discrete coupled EG method reads as follows: At the initial time $t = 0$, we take

$$\mathbf{u}_h^0 = \Pi_h^{\mathbf{u}} \mathbf{u}^0 \quad \text{and} \quad p_h^0 = \Pi_h^p p^0, \tag{8}$$

where the interpolation operators $\Pi_h^{\mathbf{u}}$ and Π_h^p are introduced in Sect. 6. Then, given $(\mathbf{u}_h^n, p_h^n) \in \boldsymbol{\mathcal{V}_h} \times \mathcal{W}_h$ with $0 \le n \le N-1$, find $(\mathbf{u}_h^{n+1}, p_h^{n+1}) \in \boldsymbol{\mathcal{V}_h} \times \mathcal{W}_h$ such that

$$\mathbf{a}_h^{\mathbf{u}}(\mathbf{u}_h^{n+1}, \mathbf{v}) - \mathbf{b}_h(\mathbf{v}, p_h^{n+1}) = \mathbf{g}_h^u(t^{n+1}; \mathbf{v}) \quad \forall \mathbf{v} \in \boldsymbol{\mathcal{V}_h}, \tag{9a}$$

$$\mathbf{c}_h\left(\frac{p_h^{n+1} - p_h^n}{\Delta t}, w\right) + \mathbf{b}_h\left(\frac{\mathbf{u}_h^{n+1} - \mathbf{u}_h^n}{\Delta t}, w\right) + \mathbf{a}_h^p(p_h^{n+1}, w) = \mathbf{g}_h^p(t^{n+1}; w) \quad \forall w \in \mathcal{W}_h, \tag{9b}$$

where

$$\begin{aligned}
\mathbf{a}_h^{\mathbf{u}}(\mathbf{v}, \mathbf{w}) &:= 2\mu(\boldsymbol{\epsilon}(\mathbf{v}), \boldsymbol{\epsilon}(\mathbf{w}))_{\mathcal{T}_h} + \lambda(\nabla \cdot \mathbf{v}, \nabla \cdot \mathbf{w})_{\mathcal{T}_h} - \langle\{\boldsymbol{\sigma}(\mathbf{v})\mathbf{n}_e\}, [\![\mathbf{w}]\!]\rangle_{\mathcal{E}_h^I \cup \Gamma_d} \\
&\quad + \theta^{\mathbf{u}}\langle[\![\mathbf{v}]\!], \{\boldsymbol{\sigma}(\mathbf{w})\mathbf{n}_e\}\rangle_{\mathcal{E}_h^I \cup \Gamma_d} + \beta^{\mathbf{u}}\left\langle h_e^{-1}[\![\mathbf{v}]\!], [\![\mathbf{w}]\!]\right\rangle_{e \in \mathcal{E}_h^I \cup \Gamma_d}, \\
\mathbf{a}_h^p(q, w) &:= (\mathbf{K}\nabla q, \nabla w)_{\mathcal{T}_h} - \langle\{\mathbf{K}\nabla q \cdot \mathbf{n}_e\}, [\![w]\!]\rangle_{\mathcal{E}_h^I \cup \Gamma_p} + \theta^p\langle\{\mathbf{K}\nabla w \cdot \mathbf{n}_e\}, [\![q]\!]\rangle_{\mathcal{E}_h^I \cup \Gamma_p} \\
&\quad + \beta^p\left\langle h_e^{-1}[\![q]\!], [\![w]\!]\right\rangle_{\mathcal{E}_h^I \cup \Gamma_p}, \\
\mathbf{b}_h(\mathbf{v}, w) &:= \alpha(\nabla \cdot \mathbf{v}, w)_{\mathcal{T}_h} - \alpha\langle\{w\}, [\![\mathbf{v}]\!] \cdot \mathbf{n}_e\rangle_{\mathcal{E}_h^I \cup \Gamma_d}, \\
\mathbf{c}_h(q, w) &:= c_0(q, w)_{\mathcal{T}_h} + \gamma^p h^2(\nabla q, \nabla w)_{\mathcal{T}_h}, \\
\mathbf{g}_h^{\mathbf{u}}(t; \mathbf{v}) &:= (\mathbf{f}(t), \mathbf{v})_{\mathcal{T}_h} + \langle\mathbf{t}_N(t), \mathbf{v}\rangle_{\Gamma_t} + \theta^{\mathbf{u}}\langle\mathbf{u}_D(t), \boldsymbol{\sigma}(\mathbf{v})\mathbf{n}_e\rangle_{\Gamma_d} + \beta^{\mathbf{u}}\left\langle h_e^{-1}\mathbf{u}_D(t), \mathbf{v}\right\rangle_{\Gamma_d}, \\
\mathbf{g}_h^p(t; w) &:= (g(t), w)_{\mathcal{T}_h} + \langle q_N(t), w\rangle_{\Gamma_f} - \alpha\langle w, (\mathbf{u}_D)_t(t) \cdot \mathbf{n}_e\rangle_{\Gamma_d} \\
&\quad + \theta^p\langle\mathbf{K}\nabla w \cdot \mathbf{n}_e, p_D(t)\rangle_{\Gamma_p} + \beta^p\left\langle h_e^{-1}p_D(t), w\right\rangle_{\Gamma_p}.
\end{aligned}$$

Here, $h_e = |e|^{\frac{1}{d-1}}$ and $\beta^{\mathbf{u}}, \beta^p$ are penalty parameters, which are assumed to be positive constants, and $\gamma^p > 0$ is a stabilization parameter. Also, $\theta^{\mathbf{u}}$ and θ^p are symmetrization parameters and chosen from $\{-1, 0, 1\}$. These three parameters lead to a symmetric interior penalty Galerkin (SIPG) method, an incomplete interior penalty Galerkin (IIPG) method, and a non-symmetric interior penalty Galerkin (NIPG) method, respectively. There are 9 possible

combinations of $\theta^{\mathbf{u}}$ and θ^p. However, in this paper, we consider only $(\theta^{\mathbf{u}}, \theta^p) = (-1, -1)$, that is, the SIPG method.

Remark 1 The bilinear form $\mathbf{c}_h\left(\frac{p_h^{n+1}-p_h^n}{\Delta t}, w\right)$ in the flow problem (9b) includes a stabilization term

$$\gamma^p h^2 \left(\nabla\left(\frac{p_h^{n+1}-p_h^n}{\Delta t}\right), \nabla w\right)_{\mathcal{T}_h}, \tag{10}$$

which is employed to satisfy the (weak) inf-sup stability condition. This same stabilization term was utilized for the Stokes problem [10] and poromechanics [11, 40] to stabilize the pressure oscillations. This term has been known as the fluid pressure Laplacian (FPL) stabilization term.

5 Local Mass Conservation

One of the interesting properties of our coupled EG method is the conservation of mass on each mesh element. Let $\mathbf{q} = -\mathbf{K}\nabla p$. Then, the integration of the mass conservation Eq. (1b) on $K \in \mathcal{T}_h$ with $\partial K \cap \partial\Omega = \emptyset$ yields

$$\langle \mathbf{q}\cdot\mathbf{n}_K, 1\rangle_{\partial K} = (g - c_0 p_t - \alpha\nabla\cdot\mathbf{u}_t, 1)_K = (g - c_0 p_t, 1)_K - \langle \alpha\mathbf{u}_t\cdot\mathbf{n}_K, 1\rangle_{\partial K}, \tag{11}$$

where $\mathbf{n}_K$ is the outward unit normal vector to ∂K. To see that our coupled EG method can mimic this identity, let us fix an interior mesh element K and take $w = 1$ on K and $w = 0$ elsewhere in (9b). Then, using the fact that $\nabla w = 0$, we get

$$c_0\left(\frac{p_h^{n+1}-p_h^n}{\Delta t}, 1\right)_K + \alpha\left(\nabla\cdot\left(\frac{\mathbf{u}_h^{n+1}-\mathbf{u}_h^n}{\Delta t}\right), 1\right)_K - \alpha\left\langle\frac{1}{2}, \left[\!\left[\left(\frac{\mathbf{u}_h^{n+1}-\mathbf{u}_h^n}{\Delta t}\right)\cdot\mathbf{n}_e\right]\!\right]\right\rangle_{\partial K}$$
$$-\langle\left\{\mathbf{K}\nabla p_h^{n+1}\cdot\mathbf{n}_K\right\}, 1\rangle_{\partial K} + \beta^p\left\langle h_e^{-1}\left[\!\left[p_h^{n+1}\right]\!\right], 1\right\rangle_{\partial K} = (g^{n+1}, 1)_K.$$

Applying the divergence theorem to the second term and combining it with the third term above, we arrive at

$$-\langle\left\{\mathbf{K}\nabla p_h^{n+1}\cdot\mathbf{n}_K\right\}, 1\rangle_{\partial K} + \beta^p\left\langle h_e^{-1}\left[\!\left[p_h^{n+1}\right]\!\right], 1\right\rangle_{\partial K}$$
$$= (g^{n+1}, 1)_K - c_0\left(\frac{p_h^{n+1}-p_h^n}{\Delta t}, 1\right)_K - \alpha\left\langle\left\{\left(\frac{\mathbf{u}_h^{n+1}-\mathbf{u}_h^n}{\Delta t}\right)\cdot\mathbf{n}_K\right\}, 1\right\rangle_{\partial K}.$$

Hence, if we define our numerical (normal) flux $\mathbf{q}_h^{n+1}$ on ∂K by

$$\mathbf{q}_h^{n+1}\cdot\mathbf{n}_K = -\left\{\mathbf{K}\nabla p_h^{n+1}\cdot\mathbf{n}_K\right\} + \beta^p h_e^{-1}\left[\!\left[p_h^{n+1}\right]\!\right],$$

we have the following local mass conservation, which is a discrete counterpart of (11):

$$\left\langle\mathbf{q}_h^{n+1}\cdot\mathbf{n}_K, 1\right\rangle_{\partial K} = (g^{n+1}, 1)_K - c_0\left(\frac{p_h^{n+1}-p_h^n}{\Delta t}, 1\right)_K - \alpha\left\langle\left\{\left(\frac{\mathbf{u}_h^{n+1}-\mathbf{u}_h^n}{\Delta t}\right)\cdot\mathbf{n}_K\right\}, 1\right\rangle_{\partial K}.$$

Note that this local mass conservation is achieved independently of the stabilization parameter γ^p.

6 Existence and Uniqueness

This sections considers the existence and uniqueness of the solution of the fully-discrete problem (9) at each discrete time t^n, $n = 1, \cdots, N$. Let us introduce the following energy norms in the EG finite element spaces $\boldsymbol{\mathcal{V}_h}$ and $\mathcal{W}_h$:

$$\|\mathbf{v}\|_{\mathcal{V}} = \left(\|\boldsymbol{\epsilon}(\mathbf{v})\|_0^2 + \beta^{\mathbf{u}}\|h_e^{-1/2}[\![\mathbf{v}]\!]\|_{L^2(\mathcal{E}_h)}^2\right)^{\frac{1}{2}} \quad \forall \mathbf{v} \in \boldsymbol{\mathcal{V}_h},$$

$$\|w\|_{\mathcal{W}} = \left(\|\nabla w\|_0^2 + \beta^{p}\|h_e^{-1/2}[\![w]\!]\|_{L^2(\mathcal{E}_h)}^2\right)^{\frac{1}{2}} \quad \forall w \in \mathcal{W}_h,$$

and a semi-norm

$$|w|_* = \sqrt{\gamma^p} h \|\nabla w\|_{L^2(\mathcal{T}_h)} \quad \forall w \in \mathcal{W}_h.$$

The following lemmas show the continuity of the bilinear forms $\mathbf{a}_h^{\mathbf{u}}(\cdot,\cdot)$, $\mathbf{a}_h^{p}(\cdot,\cdot)$, $\mathbf{b}_h(\cdot,\cdot)$, and $\mathbf{c}_h(\cdot,\cdot)$.

Lemma 1 *There exists a constant $C_{a_{\mathbf{u}}} > 0$ independent of h such that*

$$\mathbf{a}_h^{\mathbf{u}}(\mathbf{v},\mathbf{w}) \le C_{a_{\mathbf{u}}}\|\mathbf{v}\|_{\mathcal{V}}\|\mathbf{w}\|_{\mathcal{V}} \quad \forall (\mathbf{v},\mathbf{w}) \in [H^1(\mathcal{T}_h)]^d \times [H^1(\mathcal{T}_h)]^d. \tag{12}$$

Proof The result is obtained by using the Cauchy–Schwarz and Young's inequalities, the trace inequality (5), and the fact that $\|\nabla \cdot \mathbf{v}\|_{0,K} = \|tr(\boldsymbol{\epsilon}(\mathbf{v}))\|_{0,K} \le \sqrt{d}\|\varepsilon(\mathbf{v})\|_{0,K}$ on each $K \in \mathcal{T}_h$. □

Lemma 2 *There exists a constant $C_{a_p} > 0$ independent of h such that*

$$\mathbf{a}_h^{p}(q,w) \le C_{a_p}\|q\|_{\mathcal{W}}\|w\|_{\mathcal{W}} \quad \forall (q,w) \in H^1(\mathcal{T}_h) \times H^1(\mathcal{T}_h). \tag{13}$$

Lemma 3 *There exists a constant $C_b > 0$ independent of h such that*

$$\mathbf{b}_h(\mathbf{v},w) \le C_b\|\mathbf{v}\|_{\mathcal{V}}\|w\|_0 \quad \forall (\mathbf{v},w) \in [H^1(\mathcal{T}_h)]^d \times L^2(\Omega). \tag{14}$$

Moreover, There exists a constant $C_{\tilde{b}} > 0$ independent of h such that

$$\mathbf{b}_h(\mathbf{v},w) \le C_{\tilde{b}}\|\mathbf{v}\|_0\|w\|_{\mathcal{W}} \quad \forall (\mathbf{v},w) \in [H^1(\Omega)]^d \times H^1(\mathcal{T}_h). \tag{15}$$

Proof It is straightforward to show the continuity inequality in (14) using the Cauchy–Schwarz and trace inequalities. To prove (15), we first recall the following identity

$$\begin{aligned}(\nabla\cdot\mathbf{v},w)_{\mathcal{T}_h} = {}& \langle[\![\mathbf{v}]\!]\cdot\mathbf{n}_e,\{w\}\rangle_{\mathcal{E}_h} + \langle\{\mathbf{v}\}\cdot\mathbf{n}_e,[\![w]\!]\rangle_{\mathcal{E}_h^I} \\ & -(\mathbf{v},\nabla w)_{\mathcal{T}_h} \quad \forall (\mathbf{v},w) \in [H^1(\mathcal{T}_h)]^d \times H^1(\mathcal{T}_h)\end{aligned}$$

and that the average and jump operators are the same on the boundary edges. Then,

$$\mathbf{b}_h(\mathbf{v},w) = \alpha(\nabla\cdot\mathbf{v},w)_{\mathcal{T}_h} - \alpha\langle\{w\},[\![\mathbf{v}]\!]\cdot\mathbf{n}_e\rangle_{\mathcal{E}_h^I\cup\Gamma_d} = -\alpha(\mathbf{v},\nabla w)_{\mathcal{T}_h} + \alpha\langle[\![w]\!],\{\mathbf{v}\}\cdot\mathbf{n}_e\rangle_{\mathcal{E}_h^I\cup\Gamma_t}.$$

Therefore, we obtain the result by using the Cauchy–Schwarz and Young's inequalities and the trace inequality (5). □

We also have the following coercivity results for the bilinear forms $\mathbf{a}_h^{\mathbf{u}}(\cdot,\cdot)$ and $\mathbf{a}_h^{p}(\cdot,\cdot)$, which are found in [48] and [20], respectively.

Lemma 4 *(Coercivity of $\mathbf{a}_h^{\mathbf{u}}$) Assuming $\beta^{\mathbf{u}}$ is sufficiently large, there exists a constant $\kappa_{\mathbf{u}} > 0$ such that*

$$\mathbf{a}_h^{\mathbf{u}}(\mathbf{v}, \mathbf{v}) \geq \kappa_{\mathbf{u}} \|\mathbf{v}\|_{\mathcal{V}}^2 \quad \forall \mathbf{v} \in \boldsymbol{\mathcal{V}}_{\boldsymbol{h}}. \tag{16}$$

Lemma 5 *(Coercivity of $\mathbf{a}_h^{p}$) Assuming β^{p} is sufficiently large, there exists a constant $\kappa_{p} > 0$ such that*

$$\mathbf{a}_h^{p}(w, w) \geq \kappa_{p} \|w\|_{\mathcal{W}}^2 \quad \forall w \in \mathcal{W}_h. \tag{17}$$

Another key ingredient for the proof of the existence and uniqueness of the solution is the (weak) discrete inf-sup condition. This condition is particularly important to prove the locking-free property of our method even when $c_0 = 0$ and $\mathbf{K}$ and Δt are small. To this end, consider two interpolation operators $\Pi_h^{\mathbf{u}} : [H^1(\Omega)]^d \to \boldsymbol{\mathcal{V}}_{\boldsymbol{h}}$ and $\Pi_h^{p} : H^1(\Omega) \to \mathcal{W}_h$ defined in [48, Section 4] and [20], respectively. Here, we only state their useful properties and error estimates.

Lemma 6 *There exists an interpolation operator $\Pi_h^{\mathbf{u}} : [H^1(\Omega)]^d \to \boldsymbol{\mathcal{V}}_{\boldsymbol{h}}$ that satisfies*

$$(\nabla \cdot (\mathbf{v} - \Pi_h^{\mathbf{u}}\mathbf{v}), 1)_K = 0 \qquad \forall K \in \mathcal{T}_h, \tag{18a}$$

$$|\mathbf{v} - \Pi_h^{\mathbf{u}}\mathbf{v}|_j \leq C h^{m-j} |\mathbf{v}|_m, \ 0 \leq j \leq m \leq 2 \qquad \forall \mathbf{v} \in [H^2(\Omega)]^d, \tag{18b}$$

$$|\nabla \cdot (\mathbf{v} - \Pi_h^{\mathbf{u}}\mathbf{v})|_j \leq C h^{1-j} |\nabla \cdot \mathbf{v}|_1 \qquad \forall \mathbf{v} \in [H^2(\Omega)]^d, \tag{18c}$$

$$\|\Pi_h^{\mathbf{u}}\mathbf{v}\|_{\mathcal{V}} \leq C \|\mathbf{v}\|_1 \qquad \forall \mathbf{v} \in [H^1_{0,\Gamma_d}(\Omega)]^d, \tag{18d}$$

$$\|\mathbf{v} - \Pi_h^{\mathbf{u}}\mathbf{v}\|_{\mathcal{V}} \leq C h^{m-1} \|\mathbf{v}\|_m, \ 1 \leq m \leq 2 \qquad \forall \mathbf{v} \in [H^2(\Omega)]^d, \tag{18e}$$

where $C > 0$ is a generic constant independent of h.

Lemma 7 *There exists an interpolation operator $\Pi_h^{p} : H^1(\Omega) \to \mathcal{W}_h$ that satisfies*

$$(w - \Pi_h^{p} w, 1)_K = 0 \qquad \forall K \in \mathcal{T}_h, \tag{19a}$$

$$|w - \Pi_h^{p} w|_j \leq C h^{m-j} |w|_m, \ 0 \leq j \leq m \leq 2 \qquad \forall w \in H^2(\Omega). \tag{19b}$$

Lemma 8 *(Inf-sup condition) Provided that $\beta^{\mathbf{u}} > 0$ is sufficiently large, there exists a positive constant $C^* > 0$ such that*

$$C^* \|w\|_0 \leq \sup_{\mathbf{v} \in \boldsymbol{\mathcal{V}}_{\boldsymbol{h}} \setminus \{\mathbf{0}\}} \frac{\mathbf{b}_h(\mathbf{v}, w)}{\|\mathbf{v}\|_{\mathcal{V}}} + |w|_* \quad \forall w \in \mathcal{W}_h. \tag{20}$$

Proof For any nonzero $w \in \mathcal{W}_h$, w has a decomposition $w = w_c + w_d \in \mathcal{C}_h + \mathcal{D}_h^p$. Also, there exists $\tilde{\mathbf{v}} \in [H^1_{0,\Gamma_d}(\Omega)]^d$ [13] such that

$$\nabla \cdot \tilde{\mathbf{v}} = w, \quad \text{and} \quad \|\tilde{\mathbf{v}}\|_1 \leq C \|w\|_0. \tag{21}$$

Let $\mathcal{P}_h : H^1(\mathcal{T}_h) \to \mathcal{D}_h^p$ be the local L^2-projection onto the piecewise constant space. Then, we have

$$\|q - \mathcal{P}_h q\|_{0,K} \leq C h_K \|\nabla q\|_{0,K} \leq C h \|\nabla q\|_{0,K} \quad \forall q \in H^1(\mathcal{T}_h).$$

Then, using the Cauchy–Schwarz and Young's inequalities, trace inequality in (5), the properties of $\Pi_h^{\mathbf{u}}$ in (18a) and (18d), and (21), we have

$$
\begin{aligned}
\alpha\|w\|_0^2 &= \alpha(w_c + w_d, \nabla\cdot\tilde{\mathbf{v}})_{\mathcal{T}_h}\\
&= \alpha(w_c, \nabla\cdot\tilde{\mathbf{v}})_{\mathcal{T}_h} + \alpha(w_d, \nabla\cdot\Pi_h^{\mathbf{u}}\tilde{\mathbf{v}})_{\mathcal{T}_h}\\
&= \alpha(w, \nabla\cdot\Pi_h^{\mathbf{u}}\tilde{\mathbf{v}})_{\mathcal{T}_h} + \alpha(w_c, \nabla\cdot(\tilde{\mathbf{v}} - \Pi_h^{\mathbf{u}}\tilde{\mathbf{v}}))_{\mathcal{T}_h}\\
&= \mathbf{b}_h(\Pi_h^{\mathbf{u}}\tilde{\mathbf{v}}, w) + \alpha\langle\{w\}, [\![\Pi_h^{\mathbf{u}}\tilde{\mathbf{v}}]\!]\cdot\mathbf{n}_e\rangle_{\mathcal{E}_h^I\cup\Gamma_d} + \alpha(w_c - \mathcal{P}_h w_c, \nabla\cdot(\tilde{\mathbf{v}} - \Pi_h^{\mathbf{u}}\tilde{\mathbf{v}}))_{\mathcal{T}_h}\\
&= \mathbf{b}_h(\Pi_h^{\mathbf{u}}\tilde{\mathbf{v}}, w) + \alpha\langle\{w\}\mathbf{n}_e, [\![\Pi_h^{\mathbf{u}}\tilde{\mathbf{v}}]\!]\rangle_{\mathcal{E}_h^I\cup\Gamma_d} + \alpha(w_c - \mathcal{P}_h w_c, \nabla\cdot\tilde{\mathbf{v}})_{\mathcal{T}_h}\\
&\le \frac{\mathbf{b}_h(\Pi_h^{\mathbf{u}}\tilde{\mathbf{v}}, w)}{\|\Pi_h^{\mathbf{u}}\tilde{\mathbf{v}}\|_{\mathcal{V}}}\|\Pi_h^{\mathbf{u}}\tilde{\mathbf{v}}\|_{\mathcal{V}} + \alpha\|h_e^{1/2}\{w\}\mathbf{n}_e\|_{L^2(\mathcal{E}_h^I\cup\Gamma_d)}\|h_e^{-1/2}[\![\Pi_h^{\mathbf{u}}\tilde{\mathbf{v}}]\!]\|_{L^2(\mathcal{E}_h^I\cup\Gamma_d)}\\
&\quad + \alpha\|w_c - \mathcal{P}_h w_c\|_0\|\nabla\cdot\tilde{\mathbf{v}}\|_0\\
&\le \left(\sup_{\mathbf{v}\in\boldsymbol{\mathcal{V}}_h,\mathbf{v}\neq\mathbf{0}}\frac{\mathbf{b}_h(\mathbf{v}, w)}{\|\tilde{\mathbf{v}}\|_{\mathcal{V}}}\right)\|\Pi_h^{\mathbf{u}}\tilde{\mathbf{v}}\|_{\mathcal{V}} + C\left(\frac{\alpha}{\sqrt{\beta^{\mathbf{u}}}}\|w\|_0\|\Pi_h^{\mathbf{u}}\tilde{\mathbf{v}}\|_{\mathcal{V}} + \sqrt{\gamma^p}h\|\nabla w_c\|_0\|\tilde{\mathbf{v}}\|_1\right)\\
&\le C_1\left(\sup_{\mathbf{v}\in\boldsymbol{\mathcal{V}}_h,\mathbf{v}\neq\mathbf{0}}\frac{\mathbf{b}_h(\mathbf{v}, w)}{\|\mathbf{v}\|_{\mathcal{V}}} + |w|_*\right)\|w\|_0 + C_2\frac{\alpha}{\sqrt{\beta^{\mathbf{u}}}}\|w\|_0^2,
\end{aligned}
$$

where C_1 and C_2 are some positive constants. Moving the second term on the right side to the left, we arrive at

$$
\alpha\left(1 - \frac{C_2}{\sqrt{\beta^{\mathbf{u}}}}\right)\|w\|_0^2 \le C_1\left(\sup_{\mathbf{v}\in\boldsymbol{\mathcal{V}}_h,\mathbf{v}\neq\mathbf{0}}\frac{\mathbf{b}_h(\mathbf{v}, w)}{\|\mathbf{v}\|_{\mathcal{V}}} + |w|_*\right)\|w\|_0.
$$

If $\beta^{\mathbf{u}}$ is large enough, the coefficient on the left-hand side is positive. Therefore, the inf-sup condition (20) follows by letting $C^* = \frac{\alpha}{C_1}\left(1 - \frac{C_2}{\sqrt{\beta^{\mathbf{u}}}}\right)$. □

We are now ready to prove the existence and uniqueness of the solution of the new coupled EG method (9). In particular, we will show that this result is true even in the limiting case of $c_0 = 0$ and $\mathbf{K}\Delta t \to 0$, which are known to contribute to the pressure locking in poroelasticity.

Lemma 9 *Given* $(\mathbf{u}_h^n, p_h^n)$, $0 \le n \le N-1$, *there exists a unique solution* $(\mathbf{u}_h^{n+1}, p_h^{n+1})$ *to the fully-discrete coupled EG method (9).*

Proof Thanks to the finite dimensionality, the existence and uniqueness of the solution are equivalent. Therefore, it suffices to prove that the only solution to the problem (9) with $(\mathbf{u}_h^n, p_h^n) = (\mathbf{0}, 0)$, $\mathbf{g}_h^u(t^{n+1}; \mathbf{v}) = 0$, $\mathbf{g}_h^p(t^{n+1}; w) = 0$ is $(\mathbf{u}_h^{n+1}, p_h^{n+1}) = (\mathbf{0}, 0)$. That is, we want to show that the following system has only the homogeneous solution:

$$
\mathbf{a}_h^{\mathbf{u}}(\mathbf{u}_h^{n+1}, \mathbf{v}) - \mathbf{b}_h(\mathbf{v}, p_h^{n+1}) = 0 \qquad \forall\mathbf{v}\in\boldsymbol{\mathcal{V}}_h, \tag{22a}
$$

$$
\mathbf{c}_h(p_h^{n+1}, w) + \mathbf{b}_h(\mathbf{u}_h^{n+1}, w) + \Delta t\mathbf{a}_h^p(p_h^{n+1}, w) = 0 \qquad \forall w\in\mathcal{W}_h. \tag{22b}
$$

First, taking $\mathbf{v} = \mathbf{u}_h^{n+1}$ and $w = p_h^{n+1}$ in the system (22) and summing the two equations, and then using the coercivity results (16) and (17), we obtain

$$
\begin{aligned}
0 &= \mathbf{a}_h^{\mathbf{u}}\left(\mathbf{u}_h^{n+1}, \mathbf{u}_h^{n+1}\right) + \Delta t\mathbf{a}_h^p(p_h^{n+1}, p_h^{n+1}) + \mathbf{c}_h(p_h^{n+1}, p_h^{n+1})\\
&\ge \kappa_{\mathbf{u}}\|\mathbf{u}_h^{n+1}\|_{\mathcal{V}}^2 + \kappa_p\Delta t\|p_h^{n+1}\|_{\mathcal{W}}^2 + c_0\|p_h^{n+1}\|_0^2 + |p_h^{n+1}|_*^2,
\end{aligned}
$$

from which one can conclude that $\|\mathbf{u}_h^{n+1}\|_{\mathcal{V}}^2 = 0$, equivalently, $\mathbf{u}_h^{n+1} = \mathbf{0}$. On the other hand, one can draw the same conclusion for p_h^{n+1} if $c_0 \neq 0$ or $\kappa_p \Delta t$ is strictly positive. However, we are interested in the limiting case where $c_0 = 0$ and $\kappa_p \Delta t \to 0$. Therefore, we consider p_h^{n+1} separately from $\mathbf{u}_h^{n+1}$ as follows. In light of the inf-sup condition (20), there exists $\tilde{\mathbf{v}} \in \boldsymbol{\mathcal{V}_h}$ such that

$$(C^*\|p_h^{n+1}\|_0 - |p_h^{n+1}|_*)\|\tilde{\mathbf{v}}\|_{\mathcal{V}} \leq \mathbf{b}_h(\tilde{\mathbf{v}}, p_h^{n+1}). \tag{23}$$

Without loss of generality, we can assume that $\|\tilde{\mathbf{v}}\|_{\mathcal{V}} = \|p_h^{n+1}\|_0$. Now, plug $\mathbf{u}_h^{n+1} = \mathbf{0}$ and take $\mathbf{v} = \frac{C^*}{2}\tilde{\mathbf{v}}$ and $w = p_h^{n+1}$ in (22), then sum up the resulting two equations. Then, use (23), (17), and the Cauchy–Schwarz and Young's inequalities to obtain

$$\begin{aligned}
0 &= \frac{C^*}{2}\mathbf{b}_h\left(\tilde{\mathbf{v}}, p_h^{n+1}\right) + \Delta t \mathbf{a}_h^p(p_h^{n+1}, p_h^{n+1}) + \mathbf{c}_h(p_h^{n+1}, p_h^{n+1}) \\
&\geq \frac{C^*}{2}(C^*\|p_h^{n+1}\|_0 - |p_h^{n+1}|_*)\|\tilde{\mathbf{v}}\|_{\mathcal{V}} + \kappa_p \Delta t \|p_h^{n+1}\|_{\mathcal{W}}^2 + c_0\|p_h^{n+1}\|_0^2 + |p_h^{n+1}|_*^2 \\
&\geq \frac{(C^*)^2}{2}\|p_h^{n+1}\|_0^2 - \frac{C^*}{2}\left(\frac{1}{C^*}|p_h^{n+1}|_*^2 + \frac{C^*}{4}\|p_h^{n+1}\|_0^2\right) \\
&\quad + \kappa_p \Delta t \|p_h^{n+1}\|_{\mathcal{W}}^2 + c_0\|p_h^{n+1}\|_0^2 + |p_h^{n+1}|_*^2 \\
&\geq \left(\frac{3(C^*)^2}{8} + c_0\right)\|p_h^{n+1}\|_0^2 + \kappa_p \Delta t \|p_h^{n+1}\|_{\mathcal{W}}^2 + \frac{1}{2}|p_h^{n+1}|_*^2 \geq \frac{3(C^*)^2}{8}\|p_h^{n+1}\|_0^2,
\end{aligned}$$

from which $p_h^{n+1} = 0$ follows immediately regardless of the values of c_0 and $\kappa_p \Delta t$. □

Remark 2 This existence and uniqueness proof implies that there is no spurious mode in the pressure solution when $c_0, \mathbf{K}\Delta t \to 0$. Therefore, the new coupled EG method is free of pressure locking.

7 Convergence Analysis

In this section, we prove a priori error estimates for the SIPG version, *i.e.*,$(\theta^{\mathbf{u}}, \theta^p) = (-1, -1)$, of the fully-discrete problem (9). To proceed, the following regularity conditions are assumed for optimal error estimates:

$$\begin{aligned}
&p \in L^\infty(0, T_f; H^2(\Omega)), && \mathbf{u} \in L^\infty(0, T_f; [H^2(\Omega)]^d), \\
&p_t \in L^\infty(0, T_f; H^1(\Omega)), && \mathbf{u}_t \in L^\infty(0, T_f; [H^2(\Omega)]^d), \\
&p_{tt} \in L^2(0, T_f; H^1(\Omega)), && \mathbf{u}_{tt} \in L^2(0, T_f; [H^1(\Omega)]^d).
\end{aligned}$$

At any time $t > 0$, the errors $\mathbf{u} - \mathbf{u}_h$ and $p - p_h$ can be split into two parts:

$$\mathbf{u} - \mathbf{u}_h = (\mathbf{u} - \Pi_h^{\mathbf{u}}\mathbf{u}) + (\Pi_h^{\mathbf{u}}\mathbf{u} - \mathbf{u}_h) := \eta_{\mathbf{u}} + \xi_{\mathbf{u}}, \tag{24a}$$

$$p - p_h = (p - \Pi_h^p p) + (\Pi_h^p p - p_h) := \eta_p + \xi_p. \tag{24b}$$

Lemma 10 *For $\phi = \mathbf{u}$ or p, we have $\dfrac{\partial \xi_\phi}{\partial t} = \xi_{\phi_t}$ and $\dfrac{\partial \eta_\phi}{\partial t} = \eta_{\phi_t}$.*

Proof Let L be a continuous linear operator acting on continuously differentiable functions in time. Then, L and the time derivative are a commutative pair. That is, $\dfrac{\partial}{\partial t}L(f) = L\left(\dfrac{\partial f}{\partial t}\right)$.

This is particularly true for the interpolation operators $L = \Pi_h^{\mathbf{u}}$ and Π_h^p. Hence, the results follow from the definitions of ξ_ϕ and η_ϕ. □

Lemma 11 *For any scalar or vector-valued function $g \in C^2(0, T_f; H^1(\Omega))$, we have the following Taylor expansion:*

$$g^{n+1} - g^n = \Delta t\, g_t^{n+1} + \int_{t^n}^{t^{n+1}} (s - t^n) g_{tt}(s)\, ds := \Delta t\, g_t^{n+1} + \rho_{g;n+1} \tag{25}$$

and, on each element $K \in \mathcal{T}_h$,

$$\|\rho_{g;n+1}\|_{j,K} \le (\Delta t)^{\frac{3}{2}} \|g_{tt}\|_{L^2(t^n, t^{n+1}; H^j(K))}, \quad j = 0, 1, \tag{26a}$$

$$\|g^{n+1} - g^n\|_{j,K} \le \Delta t \|g_t^{n+1}\|_{j,K} + (\Delta t)^{\frac{3}{2}} \|g_{tt}\|_{L^2(t^n, t^{n+1}; H^j(K))}, \quad j = 0, 1. \tag{26b}$$

The above result is particularly true for interpolation errors.

Corollary 1 *Let $\phi = \mathbf{u}$ or p. Then,*

$$\eta_\phi^{n+1} - \eta_\phi^n = \Delta t \eta_{\phi_t}^{n+1} + \rho_{\eta_\phi;n+1} \tag{27}$$

and, on each element $K \in \mathcal{T}_h$,

$$\|\rho_{\eta_\phi;n+1}\|_{j,K} \le (\Delta t)^{\frac{3}{2}} \|\eta_{\phi_{tt}}\|_{L^2(t^n, t^{n+1}; H^j(K))}, \quad j = 0, 1, \tag{28a}$$

$$\|\eta_\phi^{n+1} - \eta_\phi^n\|_{j,K} \le \Delta t \|\eta_{\phi_t}^{n+1}\|_{j,K} + (\Delta t)^{\frac{3}{2}} \|\eta_{\phi_{tt}}\|_{L^2(t^n, t^{n+1}; H^j(K))}, \quad j = 0, 1. \tag{28b}$$

$$\begin{aligned}\|\eta_\phi^{n+1} - \eta_\phi^n\|_{\mathcal{V}} \le C \Bigg(& \frac{\Delta t}{h} \|\eta_{\phi_t}^{n+1}\|_{0,K} + \frac{(\Delta t)^{\frac{3}{2}}}{h} \|\eta_{\phi_{tt}}\|_{L^2(t^n, t^{n+1}; L^2(K))} \\ & + \Delta t \|\eta_{\phi_t}^{n+1}\|_{1,K} + (\Delta t)^{\frac{3}{2}} \|\eta_{\phi_{tt}}\|_{L^2(t^n, t^{n+1}; H^1(K))} \Bigg).\end{aligned} \tag{28c}$$

Due to the definitions of $\mathbf{u}_h^0$ and p_h^0 in (8), it is trivial to see that

$$\xi_{\mathbf{u}}^0 = 0 \quad \text{and} \quad \xi_p^0 = 0. \tag{29}$$

We are now ready to derive auxiliary error estimates. We break down this derivation into the next two lemmas.

Lemma 12 *The auxiliary errors $\xi_{\mathbf{u}}$ and ξ_p satisfy the following error equations at any time t^{n+1} with $0 \le n \le N - 1$:*

$$\mathbf{a}_h^{\mathbf{u}}(\xi_{\mathbf{u}}^{n+1}, \mathbf{v}) - \mathbf{b}_h(\mathbf{v}, \xi_p^{n+1}) = -\mathbf{a}_h^{\mathbf{u}}(\eta_{\mathbf{u}}^{n+1}, \mathbf{v}) + \mathbf{b}_h(\mathbf{v}, \eta_p^{n+1}), \tag{30a}$$

$$\begin{aligned}& \mathbf{c}_h\left(\frac{\xi_p^{n+1} - \xi_p^n}{\Delta t}, w\right) + \mathbf{b}_h\left(\frac{\xi_{\mathbf{u}}^{n+1} - \xi_{\mathbf{u}}^n}{\Delta t}, w\right) + \mathbf{a}_h^p(\xi_p^{n+1}, w) \\ & = -\mathbf{c}_h\left(\frac{\eta_p^{n+1} - \eta_p^n}{\Delta t}, w\right) - \mathbf{b}_h\left(\frac{\eta_{\mathbf{u}}^{n+1} - \eta_{\mathbf{u}}^n}{\Delta t}, w\right) - \mathbf{a}_h^p(\eta_p^{n+1}, w) \\ & \quad + c_0\left(\frac{1}{\Delta t}\rho_{p;n+1}, w\right)_{\mathcal{T}_h} + \mathbf{b}_h\left(\frac{1}{\Delta t}\rho_{\mathbf{u};n+1}, w\right) + \gamma^p h^2 \left(\frac{\nabla p^{n+1} - \nabla p^n}{\Delta t}, \nabla w\right)_{\mathcal{T}_h}.\end{aligned} \tag{30b}$$

Proof At time t^{n+1}, multiply (1a) and (1b) by $\mathbf{v} \in \boldsymbol{\mathcal{V}_h}$ and $w \in \mathcal{W}_h$, respectively, integrate by parts, then use (25) to see that the true solution $(\mathbf{u}, p)$ satisfies the following equations:

$$\mathbf{a}_h^{\mathbf{u}}(\mathbf{u}^{n+1}, \mathbf{v}) - \mathbf{b}_h(\mathbf{v}, p^{n+1}) = \mathbf{g}_h^{\mathbf{u}}(t^{n+1}; \mathbf{v}), \tag{31a}$$

$$\begin{aligned}
&\mathbf{c}_h\left(\frac{p^{n+1}-p^n}{\Delta t}, w\right) + \mathbf{b}_h\left(\frac{\mathbf{u}^{n+1}-\mathbf{u}^n}{\Delta t}, w\right) + \mathbf{a}_h^p(p^{n+1}, w) \\
&\quad = \mathbf{g}_h^p(t^{n+1}; w) + c_0\left(\frac{1}{\Delta t}\rho_{p;n+1}, w\right)_{\mathcal{T}_h} \\
&\qquad + \mathbf{b}_h\left(\frac{1}{\Delta t}\rho_{\mathbf{u};n+1}, w\right) + \gamma^p h^2\left(\frac{\nabla p^{n+1} - \nabla p^n}{\Delta t}, \nabla w\right)_{\mathcal{T}_h}.
\end{aligned} \tag{31b}$$

Subtracting (9) from (31) and using (24) and (27), we obtain the desired error equations. □

Lemma 13 *Provided that the penalty parameters $\beta^{\mathbf{u}}$ and β^p are sufficiently large, the following auxiliary error estimate holds true for any $c_0 \geq 0$:*

$$\begin{aligned}
&\max_{1\leq m\leq N}\|\xi_{\mathbf{u}}^m\|_{\mathcal{V}}^2 + c_0\max_{1\leq m\leq N}\|\xi_p^m\|_0^2 + \max_{1\leq m\leq N}|\xi_p^m|_*^2 + \Delta t\sum_{n=1}^{N}\|\xi_p^n\|_{\mathcal{W}}^2 \\
&\leq C\Big[h^2\left(\|\mathbf{u}\|_{L^\infty(0,T_f;H^2(\Omega))}^2 + \|\mathbf{u}_t\|_{L^\infty(0,T_f;H^2(\Omega))}^2\right) + (\Delta t)^2\|\mathbf{u}_{tt}\|_{L^2(0,T_f;H^1(\Omega))}^2 \\
&\quad + h^2\left(\|p\|_{L^\infty(0,T_f;H^2(\Omega)}^2 + \|p_t\|_{L^\infty(0,T_f;H^1(\Omega))}^2\right) + (\Delta t)^2(1+h^2)\|p_{tt}\|_{L^2(0,T_f;H^1(\Omega))}^2\Big],
\end{aligned} \tag{32}$$

where $C > 0$ is a generic constant independent of h and Δt.

Proof Take $\mathbf{v} = \xi_{\mathbf{u}}^{n+1} - \xi_{\mathbf{u}}^n$ in (30a) and $w = \Delta t\xi_p^{n+1}$ in (30b) and add the two resulting equations to obtain

$$\begin{aligned}
&\mathbf{a}_h^{\mathbf{u}}(\xi_{\mathbf{u}}^{n+1}, \xi_{\mathbf{u}}^{n+1} - \xi_{\mathbf{u}}^n) + \mathbf{c}_h\left(\xi_p^{n+1} - \xi_p^n, \xi_p^{n+1}\right) + \Delta t\ \mathbf{a}_h^p(\xi_p^{n+1}, \xi_p^{n+1}) \\
&\quad = -\mathbf{a}_h^{\mathbf{u}}(\eta_{\mathbf{u}}^{n+1}, \xi_{\mathbf{u}}^{n+1} - \xi_{\mathbf{u}}^n) + \mathbf{b}_h(\xi_{\mathbf{u}}^{n+1} - \xi_{\mathbf{u}}^n, \eta_p^{n+1}) - \mathbf{c}_h\left(\eta_p^{n+1} - \eta_p^n, \xi_p^{n+1}\right) \\
&\qquad - \mathbf{b}_h\left(\eta_{\mathbf{u}}^{n+1} - \eta_{\mathbf{u}}^n, \xi_p^{n+1}\right) \\
&\qquad - \Delta t\mathbf{a}_h^p(\eta_p^{n+1}, \xi_p^{n+1}) + c_0(\rho_{p;n+1}, \xi_p^{n+1})_{\mathcal{T}_h} + \mathbf{b}_h(\rho_{\mathbf{u};n+1}, \xi_p^{n+1}) \\
&\qquad + \gamma^p h^2\left(\nabla p^{n+1} - \nabla p^n, \nabla\xi_p^{n+1}\right)_{\mathcal{T}_h}.
\end{aligned} \tag{33}$$

In light of the symmetry of the bilinear forms $\mathbf{a}_h^{\mathbf{u}}$ and $\mathbf{c}_h$ and the inequality $a(a-b) \geq \frac{1}{2}(a^2 - b^2)$, we have

$$\begin{aligned}
\mathbf{a}_h^{\mathbf{u}}(\xi_{\mathbf{u}}^{n+1}, \xi_{\mathbf{u}}^{n+1} - \xi_{\mathbf{u}}^n) &\geq \frac{1}{2}(\mathbf{a}_h^{\mathbf{u}}(\xi_{\mathbf{u}}^{n+1}, \xi_{\mathbf{u}}^{n+1}) - \mathbf{a}_h^{\mathbf{u}}(\xi_{\mathbf{u}}^n, \xi_{\mathbf{u}}^n)), \\
\mathbf{c}_h(\xi_p^{n+1} - \xi_p^n, \xi_p^{n+1}) &\geq \frac{1}{2}(\mathbf{c}_h(\xi_p^{n+1}, \xi_p^{n+1}) - \mathbf{c}_h(\xi_p^n, \xi_p^n)).
\end{aligned}$$

We bound the left-hand side of (33) from below using the above inequalities, then sum over n from 0 to $m-1$ for $m \geq 1$, and further bound the left-hand side of the resulting inequality from below by making use of the coercivity of the bilinear forms $\mathbf{a}_h^{\mathbf{u}}(\cdot,\cdot)$ and $\mathbf{a}_h^p(\cdot,\cdot)$ in

Lemmas 4 and 5, respectively, to obtain

$$\frac{\kappa_{\mathbf{u}}}{2}\|\xi_{\mathbf{u}}^m\|_{\mathcal{V}}^2+\frac{c_0}{2}\|\xi_p^m\|_0^2+\frac{1}{2}|\xi_p|_*^2+\kappa_p\Delta t\sum_{n=0}^{m-1}\|\xi_p^{n+1}\|_{\mathcal{W}}^2\le\sum_{i=1}^{8}\mathcal{T}_i, \tag{34}$$

where

$$\begin{aligned}
\mathcal{T}_1&=-\sum_{n=0}^{m-1}\mathbf{a}_h^{\mathbf{u}}(\eta_{\mathbf{u}}^{n+1},\xi_{\mathbf{u}}^{n+1}-\xi_{\mathbf{u}}^n),\\
\mathcal{T}_2&=\sum_{n=0}^{m-1}\mathbf{b}_h(\xi_{\mathbf{u}}^{n+1}-\xi_{\mathbf{u}}^n,\eta_p^{n+1}),\\
\mathcal{T}_3&=-\sum_{n=0}^{m-1}\mathbf{c}_h\left(\eta_p^{n+1}-\eta_p^n,\xi_p^{n+1}\right),\\
\mathcal{T}_4&=-\sum_{n=0}^{m-1}\mathbf{b}_h\left(\eta_{\mathbf{u}}^{n+1}-\eta_{\mathbf{u}}^n,\xi_p^{n+1}\right),\\
\mathcal{T}_5&=-\sum_{n=0}^{m-1}\Delta t\mathbf{a}_h^p(\eta_p^{n+1},\xi_p^{n+1}),\\
\mathcal{T}_6&=\sum_{n=0}^{m-1}c_0\left(\rho_{p;n+1},\xi_p^{n+1}\right)_{\mathcal{T}_h},\\
\mathcal{T}_7&=\sum_{n=0}^{m-1}\mathbf{b}_h\left(\rho_{\mathbf{u};n+1},\xi_p^{n+1}\right),\\
\mathcal{T}_8&=\sum_{n=0}^{m-1}\gamma^p h^2\left(\nabla p^{n+1}-\nabla p^n,\nabla\xi_p^{n+1}\right)_{\mathcal{T}_h}.
\end{aligned}$$

To derive the desired error estimate, we need to bound $\mathcal{T}_i$ for $i=1,\dots,8$. In the following, $C>0$ is a generic constant independent of h and Δt, which are assumed to be less than 1. Let us bound $\mathcal{T}_1$ first. Using summation by parts and (29), we first rewrite $\mathcal{T}_1$ as

$$\mathcal{T}_1=-\mathbf{a}_h^{\mathbf{u}}(\eta_{\mathbf{u}}^m,\xi_{\mathbf{u}}^m)+\sum_{n=0}^{m-1}\mathbf{a}_h^{\mathbf{u}}(\eta_{\mathbf{u}}^{n+1}-\eta_{\mathbf{u}}^n,\xi_{\mathbf{u}}^n).$$

Using the continuity of $\mathbf{a}_h^{\mathbf{u}}$ and (18e), we can easily obtain

$$\mathbf{a}_h^{\mathbf{u}}(\eta_{\mathbf{u}}^m,\xi_{\mathbf{u}}^m)\le Ch\|\mathbf{u}^m\|_2\|\xi_{\mathbf{u}}^m\|_{\mathcal{V}}.$$

Similarly, for any $0\le n\le m-1$, we can show using the continuity of $\mathbf{a}_h^{\mathbf{u}}$, (28c), and (18b) that

$$\begin{aligned}
\mathbf{a}_h^{\mathbf{u}}(\eta_{\mathbf{u}}^{n+1}-\eta_{\mathbf{u}}^n,\xi_{\mathbf{u}}^n)&\le C_{a_u}\|\eta_{\mathbf{u}}^{n+1}-\eta_{\mathbf{u}}^n\|_{\mathcal{V}}\|\xi_{\mathbf{u}}^n\|_{\mathcal{V}}\\
&\le C\Delta t\left(h\|\mathbf{u}_t^{n+1}\|_2+(\Delta t)^{\frac{1}{2}}\|\mathbf{u}_{tt}\|_{L^2(t^n,t^{n+1};H^1(\Omega))}\right)\|\xi_{\mathbf{u}}^n\|_{\mathcal{V}}.
\end{aligned}$$

Now, combining the above bounds and using Young's inequality, we get

$$\begin{aligned}
\mathcal{T}_1 &\le C\left(h\|\mathbf{u}^m\|_2\|\xi_{\mathbf{u}}^m\|_{\mathcal{V}} + \Delta t\sum_{n=0}^{m-1}\left(h\|\mathbf{u}_t^{n+1}\|_2 + (\Delta t)^{\frac{1}{2}}\|\mathbf{u}_{tt}\|_{L^2(t^n,t^{n+1};H^1(\Omega))}\right)\|\xi_{\mathbf{u}}^n\|_{\mathcal{V}}\right)\\
&\le \frac{\kappa_{\mathbf{u}}}{8}\|\xi_{\mathbf{u}}^m\|_{\mathcal{V}}^2 + C\left(\Delta t\sum_{n=0}^{m-1}\|\xi_{\mathbf{u}}^n\|_{\mathcal{V}}^2 + h^2\|\mathbf{u}^m\|_2^2\right.\\
&\quad \left. + h^2\Delta t\sum_{n=0}^{m-1}\|\mathbf{u}_t^{n+1}\|_2^2 + (\Delta t)^2\sum_{n=0}^{m-1}\|\mathbf{u}_{tt}\|^2_{L^2(t^n,t^{n+1};H^1(\Omega))}\right)\\
&\le \frac{\kappa_{\mathbf{u}}}{8}\|\xi_{\mathbf{u}}^m\|_{\mathcal{V}}^2 + C\left(\Delta t\sum_{n=0}^{m-1}\|\xi_{\mathbf{u}}^n\|_{\mathcal{V}}^2 + h^2\left(\|\mathbf{u}\|^2_{L^\infty(0,T_f;H^2(\Omega))} + \|\mathbf{u}_t\|^2_{L^\infty(0,T_f;H^2(\Omega))}\right)\right.\\
&\quad \left. + (\Delta t)^2\|\mathbf{u}_{tt}\|^2_{L^2(0,T_f;H^1(\Omega))}\right).
\end{aligned}$$

To bound $\mathcal{T}_2$, we rewrite it using summation by parts and (29) as we did for $\mathcal{T}_1$. Then, use (14) and Young's inequality to see

$$\begin{aligned}
\mathcal{T}_2 &= \sum_{n=0}^{m-1}\mathbf{b}_h(\xi_{\mathbf{u}}^{n+1} - \xi_{\mathbf{u}}^n, \eta_p^{n+1}) = \mathbf{b}_h(\xi_{\mathbf{u}}^m, \eta_p^m) - \sum_{n=0}^{m-1}\mathbf{b}_h(\xi_{\mathbf{u}}^n, \eta_p^{n+1} - \eta_p^n)\\
&\le C_b\|\xi_{\mathbf{u}}^m\|_{\mathcal{V}}\|\eta_p^m\|_0 + C_b\sum_{n=0}^{m-1}\|\xi_{\mathbf{u}}^n\|_{\mathcal{V}}\|\eta_p^{n+1} - \eta_p^n\|_0\\
&\le \frac{\kappa_{\mathbf{u}}}{8}\|\xi_{\mathbf{u}}^m\|_{\mathcal{V}}^2 + C\left(\Delta t\sum_{n=0}^{m-1}\|\xi_{\mathbf{u}}^n\|_{\mathcal{V}}^2 + \|\eta_p^m\|_0^2 + \frac{1}{\Delta t}\sum_{n=0}^{m-1}\|\eta_p^{n+1} - \eta_p^n\|_0^2\right).
\end{aligned}$$

Now, using (28b) and (19b), we obtain

$$\begin{aligned}
\mathcal{T}_2 &\le \frac{\kappa_{\mathbf{u}}}{8}\|\xi_{\mathbf{u}}^m\|_{\mathcal{V}}^2 + C\left(\Delta t\sum_{n=0}^{m-1}\|\xi_{\mathbf{u}}^n\|_{\mathcal{V}}^2 + h^2\left(\|p\|^2_{L^\infty(0,T_f;H^1(\Omega))} + \|p_t\|^2_{L^\infty(0,T_f;H^1(\Omega))}\right)\right.\\
&\quad \left. + (\Delta t)^2\|p_{tt}\|^2_{L^2(0,T_f;L^2(\Omega))}\right).
\end{aligned}$$

Bounding $\mathcal{T}_3$ makes use of the Cauchy–Schwarz and Young's inequalities, (28b), and (19b):

$$\begin{aligned}
\mathcal{T}_3 &= -\sum_{n=0}^{m-1}\left(c_0\left(\eta_p^{n+1} - \eta_p^n, \xi_p^{n+1}\right)_{\mathcal{T}_h} + \gamma^p h^2\left(\nabla(\eta_p^{n+1} - \eta_p^n), \nabla\xi_p^{n+1}\right)_{\mathcal{T}_h}\right)\\
&\le c_0\sum_{n=0}^{m-1}\|\eta_p^{n+1} - \eta_p^n\|_0\|\xi_p^{n+1}\|_0 + \gamma^p h^2\sum_{n=0}^{m-1}\|\eta_p^{n+1} - \eta_p^n\|_{H^1(\mathcal{T}_h)}\|\nabla\xi_p^{n+1}\|_0\\
&\le C\left(\Delta t\sum_{n=0}^{m-1}c_0\|\xi_p^{n+1}\|_0^2 + \Delta t\sum_{n=0}^{m-1}\gamma^p h^2\|\nabla\xi_p^{n+1}\|_0^2\right.\\
&\quad \left. + \frac{1}{\Delta t}\sum_{n=0}^{m-1}\left(\|\eta_p^{n+1} - \eta_p^n\|_0^2 + \gamma^p h^2\|\eta_p^{n+1} - \eta_p^n\|^2_{H^1(\mathcal{T}_h)}\right)\right)\\
&\le C\left(\Delta t\sum_{n=0}^{m-1}(c_0\|\xi_p^{n+1}\|_0^2 + |\xi_p^{n+1}|_*^2) + h^2\|p_t\|^2_{L^\infty(0,T_f;H^1(\Omega))} + (\Delta t)^2\|p_{tt}\|^2_{L^2(0,T_f;H^1(\Omega))}\right).
\end{aligned}$$

Next, (15) is useful when bounding $\mathcal{T}_4$:

$$\begin{aligned}\mathcal{T}_4 &= -\sum_{n=0}^{m-1} \mathbf{b}_h\left(\eta_{\mathbf{u}}^{n+1}-\eta_{\mathbf{u}}^{n}, \xi_p^{n+1}\right) \le C_{\tilde{b}} \sum_{n=0}^{m-1} \|\eta_{\mathbf{u}}^{n+1}-\eta_{\mathbf{u}}^{n}\|_0 \|\xi_p^{n+1}\|_{\mathcal{W}} \\ &\le \frac{\kappa_p}{12}\Delta t \sum_{n=0}^{m-1} \|\xi_p^{n+1}\|_{\mathcal{W}}^2 + C\frac{1}{\Delta t}\sum_{n=0}^{m-1} \|\eta_{\mathbf{u}}^{n+1}-\eta_{\mathbf{u}}^{n}\|_0^2 \\ &\le \frac{\kappa_p}{12}\Delta t \sum_{n=0}^{m-1} \|\xi_p^{n+1}\|_{\mathcal{W}}^2 + C\left(h^2\|\mathbf{u}_t\|^2_{L^\infty(0,T_f;H^1(\Omega))} + (\Delta t)^2\|\mathbf{u}_{tt}\|^2_{L^2(0,T_f;L^2(\Omega))}\right).\end{aligned}$$

To bound $\mathcal{T}_5$, we use the continuity of $\mathbf{a}_h^p(\cdot,\cdot)$ and the trace inequality to see that

$$\begin{aligned}\mathcal{T}_5 &\le C_{a_p}\Delta t \sum_{n=0}^{m-1} \|\eta_p^{n+1}\|_{\mathcal{W}}\|\xi_p^{n+1}\|_{\mathcal{W}} \\ &\le \frac{\kappa_p}{12}\Delta t \sum_{n=0}^{m-1} \|\xi_p^{n+1}\|_{\mathcal{W}}^2 + C\Delta t\sum_{n=0}^{m-1}\left(\|\eta_p^{n+1}\|^2_{H^1(\mathcal{T}_h)} + \frac{1}{h^2}\|\eta_p^{n+1}\|_0^2\right) \\ &\le \frac{\kappa_p}{12}\Delta t \sum_{n=0}^{m-1} \|\xi_p^{n+1}\|_{\mathcal{W}}^2 + Ch^2\|p\|^2_{L^\infty(0,T_f;H^2(\Omega))}.\end{aligned}$$

Bounding $\mathcal{T}_6$ is pretty straightforward, so we only state the result here.

$$\mathcal{T}_6 \le C\left(\Delta t\sum_{n=0}^{m-1} c_0\|\xi_p^{n+1}\|_0^2 + (\Delta t)^2\|p_{tt}\|^2_{L^2(0,T_f;L^2(\Omega))}\right).$$

We bound $\mathcal{T}_7$ in the same fashion as for $\mathcal{T}_4$ to get

$$\mathcal{T}_7 \le \frac{\kappa_p}{12}\Delta t \sum_{n=0}^{m-1} \|\xi_p^{n+1}\|_{\mathcal{W}}^2 + C(\Delta t)^2\|\mathbf{u}_{tt}\|^2_{L^2(0,T_f;L^2(\Omega))}.$$

Lastly, the following bound for $\mathcal{T}_8$ is a consequence of applying the Cauchy–Schwarz and Young's inequalities and using (26b).

$$\mathcal{T}_8 \le C\left(\Delta t\sum_{n=0}^{m-1}|\xi_p^{n+1}|_*^2 + h^2\left(\|p_t\|^2_{L^\infty(0,T_f;H^1(\Omega))} + (\Delta t)^2\|p_{tt}\|^2_{L^2(0,T_f;H^1(\Omega))}\right)\right).$$

Combining the above bounds for $\mathcal{T}_1,\ldots,\mathcal{T}_8$ with (34) and rearranging the terms, we obtain

$$\begin{aligned}&\frac{\kappa_{\mathbf{u}}}{4}\|\xi_{\mathbf{u}}^m\|_{\mathcal{V}}^2 + \frac{c_0}{2}\|\xi_p^m\|_0^2 + \frac{1}{2}|\xi_p^m|_*^2 + \frac{\kappa_p}{4}\Delta t\sum_{n=0}^{m-1}\|\xi_p^{n+1}\|_{\mathcal{W}} \\ &\le C\Bigg[\Delta t\sum_{n=0}^{m-1}\left(\kappa_{\mathbf{u}}\|\xi_{\mathbf{u}}^{n+1}\|_{\mathcal{V}}^2 + c_0\|\xi_p^{n+1}\|_0^2 + |\xi_p^{n+1}|_*^2\right) \\ &\quad + h^2\left(\|\mathbf{u}\|^2_{L^\infty(0,T_f;H^2(\Omega))} + \|\mathbf{u}_t\|^2_{L^\infty(0,T_f;H^2(\Omega))}\right) + (\Delta t)^2\|\mathbf{u}_{tt}\|^2_{L^2(0,T_f;H^1(\Omega))} \\ &\quad + h^2\left(\|p\|^2_{L^\infty(0,T_f;H^2(\Omega))} + \|p_t\|^2_{L^\infty(0,T_f;H^1(\Omega))}\right) + (\Delta t)^2(1+h^2)\|p_{tt}\|^2_{L^2(0,T_f;H^1(\Omega))}\Bigg],\end{aligned}$$

where $C > 0$ is independent of h and Δt. As this result holds true for any $m \ge 1$, the desired auxiliary error estimate (32) follows immediately from Gronwall's lemma. □

We now state the main theorem of this section.

Theorem 1 *Provided that the penalty parameters $\beta^{\mathbf{u}}$ and β^{p} are sufficiently large, the following auxiliary error estimate holds true for any $c_0 \geq 0$:*

$$\max_{1\leq n\leq N}\|\mathbf{u}^n-\mathbf{u}_h^n\|_{\mathcal{V}}^2+c_0\max_{1\leq n\leq N}\|p^n-p_h^n\|_0^2+\max_{1\leq n\leq N}|p^n-p_h^n|_*^2+\Delta t\sum_{n=1}^{N}\|p^n-p_h^n\|_{\mathcal{W}}^2 \quad (35)$$

$$\leq C\Big[h^2\left(\|\mathbf{u}\|^2_{L^\infty(0,T_f;H^2(\Omega))}+\|\mathbf{u}_t\|^2_{L^\infty(0,T_f;H^2(\Omega))}\right)+(\Delta t)^2\|\mathbf{u}_{tt}\|^2_{L^2(0,T_f;H^1(\Omega))} \quad (36)$$

$$+h^2\left(\|p\|^2_{L^\infty(0,T_f;H^2(\Omega))}+\|p_t\|^2_{L^\infty(0,T_f;H^1(\Omega))}\right)+(\Delta t)^2(1+h^2)\|p_{tt}\|^2_{L^2(0,T_f;H^1(\Omega))}\Big], \quad (37)$$

where $C>0$ is a generic constant independent of h and Δt.

Proof The error estimate is a result of the triangle inequality, interpolation error estimates, and the auxiliary error estimate (32). □

8 Numerical Results

In this section, we present several numerical examples to validate our theoretical results and to illustrate the good performance of our proposed scheme in various scenarios. As our convergence analysis pertains to the SIPG version ($\theta^{\mathbf{u}}=\theta^{p}=-1$) of the method, we report only the results of the SIPG method in this section. All numerical experiments were performed using the finite-element and solver library HAZmath [16].

Example 1 (Convergence for a smooth solution) First, we test the proposed method against a manufactured smooth solution to confirm the optimal convergence rates proved in Sect. 7. In a computational domain $\Omega\times\mathbb{I}=(0,1)^2\times(0,1]$, the exact solutions $\mathbf{u}=[u_1,u_2]$ and p are given as follows:

$$u_1(x,y,t)=e^{-t}\left(\sin(2\pi y)(-1+\cos(2\pi x))+\frac{1}{\mu+\lambda}\sin(\pi x)\sin(\pi y)\right),$$
$$u_2(x,y,t)=e^{-t}\left(\sin(2\pi x)(1-\cos(2\pi y))+\frac{1}{\mu+\lambda}\sin(\pi x)\sin(\pi y)\right),$$
$$p(x,y,t)=e^{-t}\sin(\pi x)\sin(\pi y).$$

The body force $\mathbf{f}$ and the source/sink g are chosen to satisfy the governing equations (1), and Dirichlet boundary conditions are imposed for both p and $\mathbf{u}$. Also, the physical parameters are set to $c_0=0.0001$, $\alpha=1$, $\mathbf{K}=1$, $\mu=1$, and $\lambda=1$, and the penalty and stabilization parameters are set to $\beta^{\mathbf{u}}=100$, $\beta^{p}=100$, and $\gamma^{p}=1$.

Numerical experiments were performed on five uniform meshes. While the mesh size h varied from $1/4$ to $1/64$, the time step size was kept to $\Delta t=0.01$. The numerical errors in the displacement and pressure were measured in appropriate norms and their convergence rates were calculated. The summary of the results presented in Table 1 show the expected optimal convergence rates.

It has been known that standard low-order numerical methods for poroelasticity tend to suffer from volumetric locking in the displacement solution for a large Lamé constant λ [46]. In order to show that our EG method is robust with respect to λ, we solved the above

Table 1 Results of the convergence study in Example 1

h	$\|\mathbf{u}-\mathbf{u}_h\|_{L^\infty(0,T_f;H^1(\mathcal{T}_h))}$	Rate	$\|p-p_h\|_{L^2(0,T_f;H^1(\mathcal{T}_h))}$	Rate
0.250000	5.1252	–	0.2911	–
0.125000	2.7903	0.963	0.1563	0.957
0.062500	1.4045	1.037	0.0736	1.120
0.031250	0.7007	1.026	0.0341	1.124
0.015625	0.3500	1.013	0.0165	1.055

Table 2 Results of the convergence study in Example 1 with $\lambda = 10^6$

h	$\|\mathbf{u}-\mathbf{u}_h\|_{L^\infty(0,T_f;H^1(\mathcal{T}_h))}$	Rate	$\|p-p_h\|_{L^2(0,T_f;H^1(\mathcal{T}_h))}$	Rate
0.250000	7.0323	0.0000	0.5987	0.0000
0.125000	4.7932	0.6069	0.3015	1.0558
0.062500	2.5488	0.9540	0.1487	1.0521
0.031250	1.0206	1.3509	0.0722	1.0583
0.015625	0.3932	1.3917	0.0352	1.0443

problem with $\lambda = 10^6$ while keeping all other parameters the same. In this case, however, we added an additional penalty term $\omega^{\mathbf{u}}\lambda^2 \left\langle h_e \left[\!\left[\nabla\cdot\mathbf{u}_h^{n+1}\right]\!\right], \left[\!\left[\nabla\cdot w\right]\!\right]\right\rangle_{\mathcal{E}_h^I}$ with $\omega^{\mathbf{u}} = 0.001$ in the bilinear form $\mathbf{a}_h^{\mathbf{u}}$. This penalty term was utilized in [48] to develop a volumetric locking-free EG method for linear elasticity. Optimal convergence rates of the method for this large λ value are demonstrated in Table 2. Though this (volumetric) locking-free property has been confirmed in several other unreported numerical experiments as well, error estimates independent of λ are yet to be derived.

Example 2 (Stabilization and eliminated pressure locking) In this example, we solve a cantilever bracket problem, one of the popular examples in the literature on poroelasticity [32, 33]. This example is to demonstrate that our coupled EG method does not suffer from pressure locking. The spatial domain is the same as in Example 1, whereas the body force $\mathbf{f}$ and the source/sink term g are set to zero in this example. The boundary conditions are summarized in Fig. 1a. As mentioned earlier, pressure locking stems from the lack of inf-sup stability condition for the problems with $c_0 = 0$ and very small $\mathbf{K}$ and/or Δt. Recall that the proposed coupled EG method employs a stabilization term to ensure the inf-sup condition. Therefore, the main purpose of this numerical example is to test the new method with and without the stabilization term and show the effect of the stabilization term concerning pressure locking. For both simulations, we used the following physical and numerical parameters, which tend to cause pressure locking:

$$\alpha = 0.93,\ c_0 = 0,\ \mathbf{K} = 10^{-9},\ \lambda = 10, \mu = 10,\ h = 1/32,\ \Delta t = 0.001,\ \beta^{\mathbf{u}} = \beta^p = 100.$$

On the other hand, we used $\gamma^p = 0.01$ and $\gamma^p = 0$ to turn on and off the stabilization term, respectively. The pressure solutions after one time step are shown in Fig. 1b and c, respectively. Pressure oscillations (locking) are visible in Fig. 1b, where the stabilization term was not used. However, no oscillations are present in Fig. 1c, where the stabilization term was used. Moreover, the magnitude of the two pressure solutions are quite different.

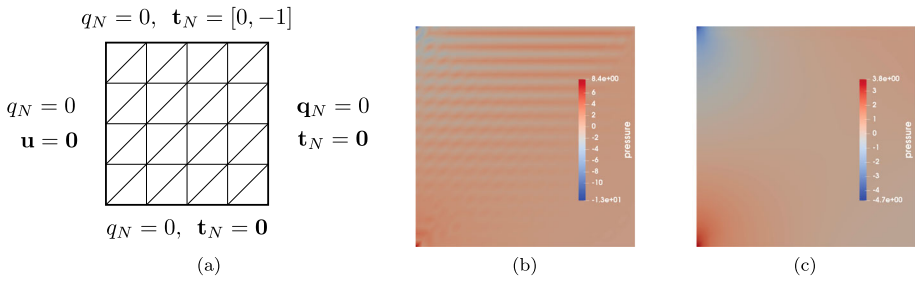

Fig. 1 **a** Example 2 setup, **b** pressure solution without a stabilization term ($\gamma^p = 0$), and **c** pressure solution with a stabilization term ($\gamma^p = 0.01$)

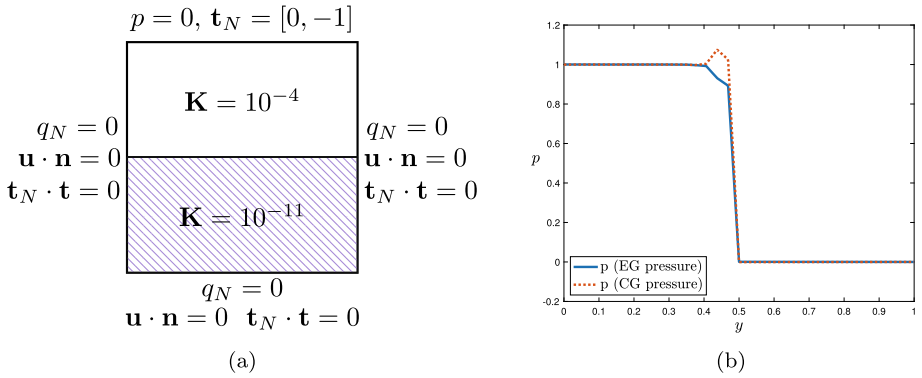

Fig. 2 **a** Example 3 setup and **b** comparisons of the pressure solutions from the coupled EG method and the coupled EG-CG method after 1000 time steps

This test clearly shows the importance of the inf-sup condition to eliminate pressure locking and that our stabilization term indeed ensures the inf-sup condition.

Example 3 (Eliminated numerical overshoots in a layered medium) The numerical experiments in this example consider the significance of using a locally conservative method for the pressure when simulating poroelasticity in a heterogeneous medium as previously investigated by others in [11, 12, 18, 19]. In the unit square $(0, 1)^2$, the permeability $\mathbf{K}$ is defined as a discontinuous function; the upper quarter of the domain ($y \geq 0.5$) has the permeability $\mathbf{K} = 10^{-4}$ and the remaining domain ($y < 0.5$) has $\mathbf{K} = 10^{-12}$ as shown in Fig. 2a. This setup represents a simple layered field with high-contrast $\mathbf{K}$ values. The boundary conditions are also summarized in Fig. 2a. In the conditions, $\mathbf{n}$ and $\mathbf{t}$ are the outward unit normal and tangential vectors, respectively. The external body force and sink/source functions are taken to be $\mathbf{f} = \mathbf{0}$ and $g = 0$.

In order to show the importance of using a locally conservative method for the flow subproblem, we compare our new EG method with a method that is not locally conservative. Specifically, the method used for comparison solves the mechanical problem with the same EG method as in (9a), but the flow equation is solved with a stabilized linear CG method with the same FPL stabilization term as in (10). It is well-known that the linear CG method with or without this stabilization term is not locally conservative. For both methods, the following physical and numerical parameters are used:

$$c_0 = 0,\ \alpha = 1,\ \lambda = 1,\ \mu = 1,\ \Delta t = 10,\ h = 1/32,\ \beta^{\mathbf{u}} = \beta^p = 10^3,\ \gamma^p = 0.1.$$

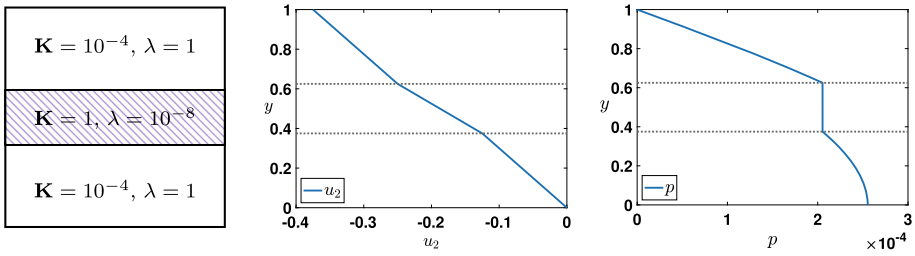

(a) Setup (b) u_2 (c) p

Fig. 3 **a** Example 4 setup and **b** displacement (u_2) and **c** pressure p solutions along the vertical line $x = 0.5$ after 1000 time steps

Figure 2b presents a comparison of the pressure, p, produced by the two methods at the final time $T_f = 10,000$. Even though the linear CG method is stabilized using the FPL stabilization method, the coupled EG-CG method still produces unphysical overshoot near the interface of the two material layers. On the contrary, our new coupled EG method produces no overshoot in the pressure solution. These results clearly show that the stabilization technique itself is not enough to eliminate numerical overshoots in a heterogeneous medium with a high-contrast permeability if the method is not locally conservative.

Example 4 (A layered medium with discontinuous λ and $\mathbf{K}$) This example concerns a layered medium with discontinuities in both λ in the mechanics problem and $\mathbf{K}$ in the flow problem. We use the same spatial domain $(0, 1)^2$, boundary conditions, the body force $\mathbf{f}$, and the source/sink function g as in Example 3. In the domain, both λ and $\mathbf{K}$ have discontinuities along the two horizontal lines $y = 0.625$ and $y = 0.375$, and their values are shown in the Fig. 3a. The rest of the physical and numerical parameters are as follows:

$$\alpha = 1,\ c_0 = 0,\ \Delta t = 10,\ h = 1/32,\ \beta^p = \beta^{\mathbf{u}} = 10^3,\ \gamma^p = 0.01.$$

Due to the boundary conditions, the solutions change only in the vertical direction. The cross sectons of the displacement (u_2) and pressure solutions along the vertical line $x = 0.5$ are presented in Fig. 3a and b. Here, we observe no unphysical oscillations near the material interfaces in either solution despite the large jumps in the λ and $\mathbf{K}$ values.

Example 5 (Poroelasticity in a random heterogeneous permeability field) In this last example, we consider a layered poroelastic medium with a randomly heterogeneous permeability field. We take the spatial domain $\Omega = (0, 10) \times (0, 2.5)$ and the final time $T_f = 100$. In this domain, the permeability values were chosen randomly from the interval $[10^{-4}, 10^{-1}]$. The layers in the medium is due to the discontinuous Lamé constant λ as shown in Fig. 4. But, other physical parameters $c_0 = 0.1$, $\alpha = 1$, and $\mu = 1$ are constant throughout the entire domain. We imposed an influx condition $q_N = 10^{-2}$ for the flow problem and a traction boundary condition $\mathbf{t}_N = [0, -10^{-7}]$ for the mechanics problem on the top boundary. On all other boundaries, we imposed the following conditions: $q_N = 0,\ \mathbf{u} \cdot \mathbf{n} = 0,$ and $\mathbf{t}_N \cdot \mathbf{t} = 0$. On the other hand, the numerical parameters used in this simulation are $h = 1/16,\ \Delta t = 1,\ \beta^{\mathbf{u}} = \beta^p = 100,$ and $\gamma^p = 0.01$.

Figure 5 illustrates the displacement and pressure solutions after 100 time steps. The horizontal displacement, u_1, is very small in the entire domain as seen in Fig. 5a. This was expected considering the imposed boundary conditions. On the other hand, the vertical displacement and pressure solutions presented in Fig. 5b and c show the effect of the discontinuous elastic property of the medium. However, its effect is less pronounced in the pressure

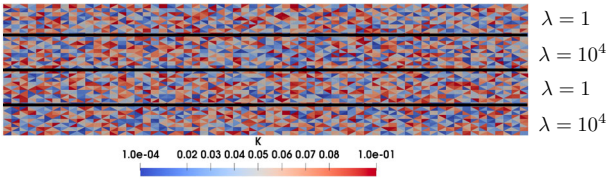

Fig. 4 Random permeability field $\mathbf{K}$ and discontinuous Lamé constant λ in Example 5

(a) u_1

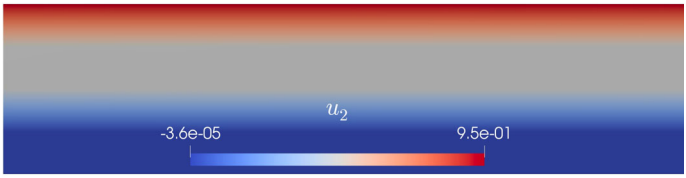

(b) u_2

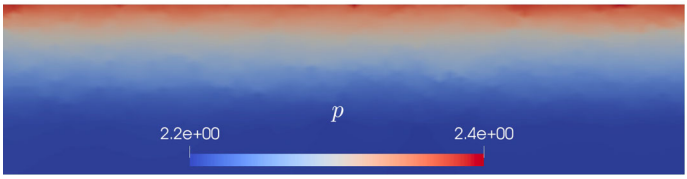

(c) p

Fig. 5 Numerical solutions at time $t = 100$ in Example 5: **a** horizontal displacement (u_1), **b** vertical displacement (u_2), and **c** pressure

solution than in u_2 as the permeability $\mathbf{K}$ is a more influencing factor than the Lamé constant λ to the flow problem. Also, we observe no unphysical oscillations in the solutions. This example demonstrates that the coupled EG method has great potential to handle problems in more realistic scenarios.

Funding The work of S. Lee was partially supported by the U.S. National Science Foundation Grant DMS-1913016 and DMS-2208402. The work of S.-Y. Yi was supported by the U.S. National Science Foundation under Grant DMS-2208426.

Data availability The datasets generated during and/or analyzed during the current study are available from the corresponding author on reasonable request.

Declarations

Conflict of interest The authors declare that they have no conflict of interest.

References

1. Adams, R.A., Fournier, J.J.: Sobolev spaces, vol. 140. Elsevier (2003)
2. Ambartsumyan, I., Khattatov, E., Yotov, I.: A coupled multipoint stress-multipoint flux mixed finite element method for the Biot system of poroelasticity. Comput. Methods Appl. Mech. Engrg. **372**, 113407 (2020)
3. Bærland, T., Lee, J.J., Mardal, K.A., Winther, R.: Weakly imposed symmetry and robust preconditioners for Biot's consolidation model. Comput. Methods Appl. Math. **17**(3), 377–396 (2017)
4. Bean, M.L., Yi, S.Y.: An immersed interface method for a 1D poroelasticity problem with discontinuous coefficients. J. Comput. Appl. Math. **272**, 81–96 (2014)
5. Biot, M.: General theory of three-dimensional consolidation. J. Appl. Phys. **12**(2), 155–164 (1941)
6. Biot, M., Willis, D.: The elastic coefficients of the theory of consolidation. J. Appl. Mech **15**, 594–601 (1957)
7. Boffi, D., Brezzi, F., Fortin, M.: Mixed finite element methods and applications, vol. 44. Springer (2013)
8. Booker, J.R., Small, J.: An investigation of the stability of numerical solutions of Biot's equations of consolidation. Int. J. Solids. Struct. **11**(7–8), 907–917 (1975)
9. Brezzi, F., Fortin, M.: Mixed and hybrid finite element methods, Springer Series in Computational Mathematics, vol. 15. Springer-Verlag, New York (1991)
10. Brezzi, F., Pitkäranta, J.: On the stabilization of finite element approximations of the Stokes equations. In: Efficient solutions of elliptic systems, pp. 11–19. Springer (1984)
11. Choo, J.: Stabilized mixed continuous/enriched Galerkin formulations for locally mass conservative poromechanics. Comput. Methods Appl. Mech. Engrg. **357**, 112568 (2019)
12. Choo, J., Lee, S.: Enriched Galerkin finite elements for coupled poromechanics with local mass conservation. Comput. Methods Appl. Mech. Engrg. **341**, 311–332 (2018)
13. Gopalakrishnan, J., Qiu, W.: Partial expansion of a Lipschitz domain and some applications. Front. Math. China **7**(2), 249–272 (2012)
14. Haga, J., Osnes, H., Langtangen, H.: On the causes of pressure oscillations in low permeable and low compressible porous media. Int. J. Numer. Anal. Methods. Geomech. **36**(12), 1507–1522 (2012)
15. Honorio, H., Maliska, C., Ferronato, M., Janna, C.: A stabilized element-based finite volume method for poroelastic problems. J. Comput. Phys. **364**, 49–72 (2018)
16. Hu, X., Adler, J., Zikatanov, L.: HAZmath: A Simple Finite Element, Graph, and Solver Library (2020). https://hazmathteam.github.io/hazmath/
17. Kadeethum, T., Lee, S., Ballarin, F., Choo, J., Nick, H.M.: A locally conservative mixed finite element framework for coupled hydro-mechanical-chemical processes in heterogeneous porous media. Comput. Geosci. **152**, 104774 (2021)
18. Kadeethum, T., Lee, S., Nick, H.: Finite element solvers for Biot's poroelasticity equations in porous media. Math. Geosci. **52**(8), 977–1015 (2020)
19. Kadeethum, T., Nick, H.M., Lee, S., Ballarin, F.: Enriched Galerkin discretization for modeling poroelasticity and permeability alteration in heterogeneous porous media. J. Comput. Phys. **427**, 110030 (2021)
20. Lee, S., Lee, Y.J., Wheeler, M.F.: A locally conservative enriched Galerkin approximation and efficient solver for elliptic and parabolic problems. SIAM J. Sci. Comput. **38**(3), A1404–A1429 (2016)
21. Lee, S., Mikelić, A., Wheeler, M.F., Wick, T.: Phase-field modeling of proppant-filled fractures in a poroelastic medium. Comput. Methods Appl. Mech. Engrg. **312**, 509–541 (2016)
22. Lee, S., Wheeler, M.F.: Adaptive enriched Galerkin methods for miscible displacement problems with entropy residual stabilization. J. Comput. Phys. **331**, 19–37 (2017)
23. Lee, S., Wheeler, M.F.: Enriched Galerkin methods for two-phase flow in porous media with capillary pressure. J. Comput. Phys. **367**, 65–86 (2018)
24. Liu, R.: Discontinuous Galerkin finite element solution for poromechanics. The University of Texas at Austin (2004)
25. Liu, R., Wheeler, M., Dawson, C., Dean, R.: On a coupled discontinuous/continuous Galerkin framework and an adaptive penalty scheme for poroelasticity problems. Comput. Methods Appl. Mech. Engrg. **198**(41–44), 3499–3510 (2009)
26. Masson, Y.J., Pride, S., Nihei, K.: Finite difference modeling of Biot's poroelastic equations at seismic frequencies. J. Geophys. Res. Solid Earth **111**, B10305 (2006). https://doi.org/10.1029/2006JB004366

27. Mercer, G., Barry, S.: Flow and deformation in poroelasticity-II numerical method. Math. Comput. Model. **30**(9–10), 31–38 (1999)
28. Murad, M., Loula, A.: On stability and convergence of finite element approximations of Biot's consolidation problem. Int. J. Numer. Methods Eng. **37**(4), 645–667 (1994)
29. Murad, M.A., Thomée, V., Loula, A.F.: Asymptotic behavior of semidiscrete finite-element approximations of Biot's consolidation problem. SIAM J. Numer. Anal. **33**(3), 1065–1083 (1996)
30. Nitsche, J.A.: On Korn's second inequality. RAIRO Anal. Numér. **15**(3), 237–248 (1981)
31. Nordbotten, J.: Cell-centered finite volume discretizations for deformable porous media. Int. J. Numer. Methods Eng. **100**(6), 399–418 (2014)
32. Phillips, P., Wheeler, M.: A coupling of mixed and continuous Galerkin finite element methods for poroelasticity. I. The continuous in time case. Comput. Geosci. **11**(2), 131–144 (2007)
33. Phillips, P., Wheeler, M.: A coupling of mixed and continuous Galerkin finite element methods for poroelasticity II: the discrete-in-time case. Comput. Geosci. **11**(2), 145–158 (2007)
34. Phillips, P., Wheeler, M.: A coupling of mixed and discontinuous Galerkin finite-element methods for poroelasticity. Comput. Geosci. **12**(4), 417–435 (2008)
35. Reed, M.: An investigation of numerical errors in the analysis of consolidation by finite elements. Int. J. Numer. Anal. Methods. Geomech. **8**(3), 243–257 (1984)
36. Rodrigo, C., Gaspar, F., Hu, X., Zikatanov, L.: Stability and monotonicity for some discretizations of the Biot's consolidation model. Comput. Methods Appl. Mech. Engrg. **298**, 183–204 (2016)
37. Showalter, R.E.: Diffusion in poro-elastic media. J. Math. Anal. Appl. **251**(1), 310–340 (2000)
38. Sokolova, I., Bastisya, M., Hajibeygi, H.: Multiscale finite volume method for finite-volume-based simulation of poroelasticity. J. Comput. Phys. **379**, 309–324 (2019)
39. Sun, S., Liu, J.: A locally conservative finite element method based on piecewise constant enrichment of the continuous Galerkin method. SIAM J. Sci. Comput. **31**(4), 2528–2548 (2009)
40. Truty, A., Zimmermann, T.: Stabilized mixed finite element formulations for materially nonlinear partially saturated two-phase media. Comput. Methods Appl. Mech. Engrg. **195**(13–16), 1517–1546 (2006)
41. Vermeer, P., Verruijt, A.: An accuracy condition for consolidation by finite elements. Int. J. Numer. Anal. Methods. Geomech. **5**(1), 1–14 (1981)
42. Wan, J.: Stabilized finite element methods for coupled geomechanics and multiphase flow. Stanford university (2003)
43. Wheeler, M., Xue, G., Yotov, I.: Coupling multipoint flux mixed finite element methods with continuous Galerkin methods for poroelasticity. Comput. Geosci. **18**(1), 57–75 (2014)
44. Yi, S.Y.: A coupling of nonconforming and mixed finite element methods for Biot's consolidation model. Numer. Methods Partial Differ. Equ. **29**(5), 1749–1777 (2013)
45. Yi, S.Y.: Convergence analysis of a new mixed finite element method for Biot's consolidation model. Numer. Methods Partial Differ. Equ. **30**(4), 1189–1210 (2014)
46. Yi, S.Y.: A study of two modes of locking in poroelasticity. SIAM J. Numer. Anal. **55**(4), 1915–1936 (2017)
47. Yi, S.Y., Hu, X., Lee, S., Adler, J.H.: An enriched Galerkin method for the Stokes equations. Comput. Math. Appl. **120**, 115–131 (2022)
48. Yi, S.Y., Lee, S., Zikatanov, L.: Locking-free enriched Galerkin method for linear elasticity. SIAM J. Numer. Anal. **60**(1), 52–75 (2022)